

Quantum state transfer: interplay between gate and readout errors

Bharat Thotakura¹ → Tzu-Chieh Wei^{1,2}

Received: 14 September 2022 / Accepted: 19 June 2023 / Published online: 6 July 2023 © The Author(s), under exclusive licence to Springer Science+Business Media, LLC, part of Springer Nature 2023

Abstract

Quantum networks consist of quantum nodes that are linked by entanglement, and quantum information can be transferred from one node to another. Operations can be applied to qubits of local nodes coordinated by classical communication to manipulate quantum states, and readout/measurement will be employed to obtain results. Here, we use quantum circuits to simulate quantum state transfer between two nodes connected in a linear geometry through other nodes. We explore the interplay between gate and readout errors on the performance of state transfer. We find that the nominal success probability is not necessarily a monotonic function of the two error rates and employ numerical simulations and analytic tools to understand their interplay.

Keywords Quantum state transfer \cdot Teleportation \cdot Swap \cdot Gate teleportation \cdot GHZ state \cdot Noise \cdot Error mitigation

1 Introduction

One of the goals of quantum technology research deals with linking up many local quantum devices to act together as a network called a quantum network or internet. The local nodes in that network (see Ref. [1]) are quantum processing units, which can be thought of as small quantum computers with quantum memory. The links connecting these nodes can be either classical or quantum channels (or both)—that is, equipped with a mechanism of communication between nodes, with the basic protocols to establish entanglements, such as quantum teleportation [2] and entanglement swapping [3].

² C. N. Yang Institute for Theoretical Physics, State University of New York, Stony Brook, NY 11794-3840, USA



Bharat Thotakura bthotakura9@gmail.com

Department of Physics and Astronomy, State University of New York, Stony Brook, NY 11794-3800, USA

In 2001, Duan, Lukin, Cirac, and Zoller (DLCZ) proposed a long-distance quantum communication protocol (i.e., the DLCZ protocol) over long lossy channels using photons and atomic ensembles [4]. Despite the scheme's simplicity, compared to the complexity of realizing a universal quantum computer, a full-scale implementation of the DLCZ protocol over long distances has not yet been carried out. However, advancements are being made, such as individual addressability of multiplexed quantum memory [5], teleportation between non-neighboring nodes [6], the distribution of a Greenberger–Horne–Zeilinger state (GHZ), and multi-node entanglement swapping (see Ref. [7]), and establishment of long-range entanglement between single atoms [8]. Other efforts include schemes and experiments for measurement-based filtration to GHZ state [9], high-fidelity multi-qubit gates for SWAP and GHZ construction with quantum hardware, such as NMR [10, 11], and remote entanglement generation and distribution towards the development of stacks of quantum networks [12–16].

As Wehner, Elkouss, and Hanson lay down in Ref. [17], all these quantum network stages and efforts coalesce into a unified framework of stages toward a quantum internet. Ultimately, we would like to reach a full quantum computation stage in the quantum network—before which we would ideally have a few-qubit fault-tolerant network. However, the current stage in the development of quantum computers is more accurately characterized as the NISQ (noisy intermediate-scale quantum) era [18], and presently, there are mostly proposals and small-scale tests of fault-tolerant quantum computation [19–23] only. Thus, the issue of noise remains one of the biggest impediments to practical and scalable quantum computation and consequently to the quality and performance of a quantum network.

In the context of the quantum internet roadmap [17], noise and errors hamper functionality in all quantum network stages of state preparation and measurement, entanglement distribution, and entanglement generation execution. In this paper, we focus on the issue of quantum state transfer [24], an important process in quantum networks, especially with regard to the entanglement swapping process in quantum repeaters—and which offers implications for the aforementioned quantum network stages. Specifically, we concern ourselves with the interaction of noise errors and their effect on a measure of successful state transfer.

Despite that quantum communication is well developed [25–27], no large-scale quantum network testbed is currently available. In contrast, there are several available quantum computers. Moreover, the usage of NISQ devices has provided ample fertile ground to test various aspects of quantum networks ranging from quantum teleportation protocols [28, 29], graph state generation [30], to testing quantum router and quantum repeater designs [31–33]. As such, our study will use qubits and gates in the NISQ context to simulate quantum state transfer. In particular, we investigate the interplay between gate and readout errors due to the importance of measurement readout of expectation values and the prevalent usage of noisy gates such as CNOT (CX) in most protocols.

There is a focus in the literature on quantum state transfer for a particular physical system and its experimental realization like a topological chain [34], solid-state quantum network [35], or spin networks [36–38] or via Huddard interaction [39], relying on some form of swapping usually. There is also an emphasis on the concept of perfect state transfer (PST) but with quantum walks [40, 41]. In comparison, we narrow our



investigation at the algorithmic scheme level, looking at how specific model schemes are affected by varying degrees of gate and readout errors. By understanding their counterintuitive error dynamics specifically and their leaking error mixing effects on measures of the fidelity for quantum state transfer, our efforts work toward the ends of designing noise-aware schemes for robust quantum networks. This can be crucial when trying to mitigate expectation values in novel ways, especially at the nominal level, to understand the error dominance, the scaling, and any error interference. Additionally, it can also offer further insight into the fragility of certain entangled states under particular noise [42] and aid in using techniques such as maximum likelihood estimation (MLE) in quantum state tomography [43]. More recent techniques such as Clifford data regression [44] are one possibility of exploiting noise-scaling, for example, and we also briefly introduce the element of using zero noise extrapolation (see Ref. [45, 46]) with predictive models on the scaled noise expectation value simulations in this work.

The remainder of this paper is organized as follows. In Sect. 2, we describe the setup of our investigation using Qiskit [47], outline the different quantum state transfer schemes we will compare throughout the paper, and address their initial performance. Then, in Sect. 3 we present several plot results from numerical Qiskit simulations of the different schemes and try to identify the interplay between gate and readout errors. We then present an analytical point of view as well that matches the results seen in the initial numerical Qiskit simulations. In Sect. 4, we touch upon the possible role error mitigation; mainly, zero-noise extrapolation can serve in our analysis. Finally, in Sect. 5, we summarize our results and propose a future outlook.

2 State transfer schemes

Due to the issue of diminishing the quality of quantum states across large distances in a quantum network, efficient and effective state storage and transfer are crucial. Even with the use of intermediary repeaters, entanglement swapping remains a significant component, and hence the problem of state transfer remains [48].

To investigate effective quantum state transfers, one can look at how different schemes, or perhaps 'resource schemes', can vary and, more intriguingly, affect the success probability of transferring an arbitrary initial state from a starting site *i* to an end site *j*. These starting and end sites would be connected via some known or provided connectivity topology that dictates the specific gate operations that are available for use, as well as the positioning of intermediary qubits facilitating the connection between the start and end sites. Given such a setup, for simplicity, we consider in this section onward a qubit mapping to a linear chain connected topology, and we ask how certain schemes would fair in achieving the goal of successful state transfer—especially under noisy and error-prone situations. Specifically, the physical setup that we consider is a collection of qubits in a quantum computer, which can be acted by single- and two-qubit gates, such as the transmon qubits of IBMQ. While still in the broader context of quantum networks, we treat them from the state transfers perspective, not across long-distance nodes but across a few qubits geometrically nearby.



275 Page 4 of 36 B. Thotakura, T.-C Wei

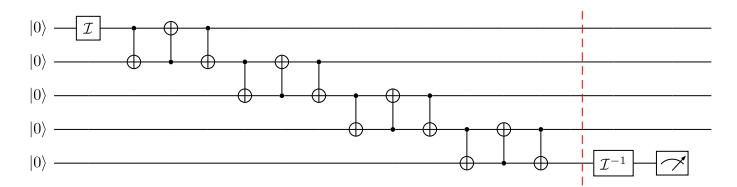


Fig. 1 An example five-qubit circuit schematic for the successive SWAP scheme. We note that the traditional SWAP gate remains in the three CNOT decomposed format [54] for all simulations done to study the impact of CNOT gate noise clearly

With that in mind, in this paper, we perform an analysis of how the following four different schemes (see Appendix A for the terminology) would fair when given such a task:

- 1. SWAP: Sole, successive state swaps from a site i to a site j;
- 2. *Teleportation*: Sole, successive state teleportation [2] (via the creation of a sequence of Bell pairs) from a site *i* to a site *j*;
- 3. *GHZ*: State transfer from site *i* to site *j* via the creation of a GHZ state [49, 50] as a channel:
- 4. *Cluster*: State transfer from a site *i* to a site *j* via the intermediate creation of a cluster state as a resource channel [51, 52], also known as gate teleportation.

Each of the four schemes considered offers some interesting variation. One uses the least measurements (SWAP scheme), one uses the most measurement-outcome-dependent gates (GHZ scheme), and another uses a well-known protocol involving Bell state measurements (teleportation scheme), while an alternative may be more suited to a particular qubit topology (cluster state resource scheme).

In terms of evaluating an event of a successful state transfer, we sample a random initial state vector in Qiskit (approximately from the uniform Haar measure) and initialize the qubit at site i (call it the first qubit w.l.o.g.) in that state using some initializing gate \mathcal{I} for all the schemes. We then apply the gates of a particular state transfer scheme, and finally, in the end, apply a so-called 'disentangler' (which we denote by \mathcal{I}^{-1}) at site j (or rather, the final qubit). This \mathcal{I}^{-1} operation is a gate in Qiskit that undoes the unitaries that initialized the first qubit into the starting random state vector used at the beginning of the circuit. Lastly, this is followed by a measurement in the Z basis to get the probability of being in our very initial $|0\rangle$ state. This probability of measuring '0' is the *nominal* success probability, and when there are errors and noise, the act of obtaining '0' does not necessarily mean that the final state before \mathcal{I}^{-1} is the same random state we begin with but only indicates that the protocol was successfully completed. (This is in some sense similar to the nominal success of the entanglement swap in the DLCZ protocol when a single photon is detected at the beam splitter [4, 53].) The particular implementation of the respective schemes is best illustrated with circuit examples, and, in the order listed above, they can be seen in Figs. 1, 2, 3 and 4 for five qubits. Additionally, a more detailed explanation of the GHZ and Cluster state schemes can be found in Appendix C. We note that to highlight and contrast any scheme advantage, we use the full set of CNOTs for the successive SWAP scheme.



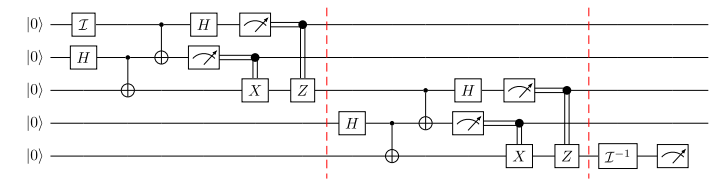


Fig. 2 An example five-qubit circuit schematic for the successive teleportation scheme. We note that the block of gates in the dashed sections form the standard teleportation protocol utilizing Bell state creation

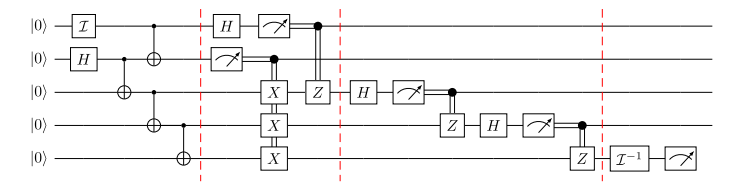


Fig. 3 An example five-qubit circuit schematic for the GHZ scheme wherein an initial GHZ state is used like a channel for state transfer from the first to the last qubit

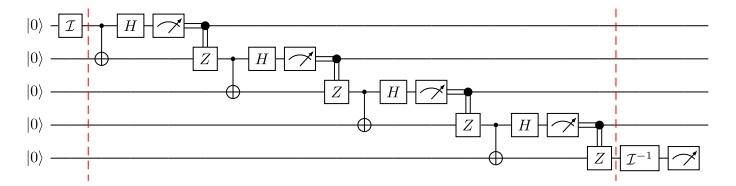


Fig. 4 An example five-qubit, simplified circuit schematic derived from using an intermediary 'resource' cluster state to facilitate state transfer in the cluster scheme. We note that in the gate teleportation used in the cluster scheme, the controlled-Z(CZ) gate is the native gate and the remaining qubits should be initialized in $|+\rangle$, but the circuit is translated to the CNOT-based circuits, as CNOT and CZ are related by Hadamard (H) gates

To start, we consider running the four schemes on Qiskit's 'QASM simulator' and applying the noise model of 'IBM Q Montreal' device (simulated via the FakeMontreal backend provider to best emulate the real device) with no circuit mapping optimization or error mitigation applied. We restrict ourselves to only the QASM simulator in this section as we are limited in running most of the schemes (that is, all but the SWAP scheme) on a real IBM device. In particular, we require the use of real-time conditional quantum gates based on measurement results (as is needed to apply the classical corrections after quantum teleportation as an example). Unfortunately, at the time of the manuscript completion and submission, the conditional 'c_if()' functionality in Qiskit could not be used on IBM's real devices as of the writing of this paper though we expect it may be a feature available in the future so that actual execution of the schemes considered here can be done and their results can be compared with 1 We could still, of course, use the principle of delayed measurements to postpone all measurements till the end, however, that introduces additional control gates that may

 $^{^{1}\,}$ Note added: This feature has become available in some of IBM's quantum devices since November 2022. But to perform the actual demonstration is beyond the scope of the current work.



not be directly available with the nearest-neighbor qubits and may cloud our analysis on any advantage certain schemes may have over each other.

In light of this, we mostly employ the 'QASM' simulator in Qiskit, as that allows us to simulate the operation of real devices and to make full use of, otherwise unavailable, measurement-outcome-based conditional gates (indicated by the double lines connecting gates in Figs. 1, 2, 3 and 4).

2.1 Noisy simulations

Given such a setup, we began simulations for each scheme ranging from three qubits to thirteen qubits (in a linear geometry) on a quantum circuit, enabling all the gate and readout error noise from the real-device noise model. The gate error model specifies the application of non-ideal quantum gate operations in a quantum circuit because of a particular probability of error. For example, with the H gate, an ideal application of the H gate on the basis states $|0\rangle$ and $|1\rangle$ results in an output of the $|+\rangle = \frac{1}{\sqrt{2}}(|0\rangle + |1\rangle)$ and $|-\rangle = \frac{1}{\sqrt{2}}(|0\rangle - |1\rangle)$ states, respectively. With the presence of a gate error model, for example, a depolarizing error model with depolarization error, p, application of the H gate on an initial state means that the ideal H gate will be applied with probability (1-p), but the state will undergo a random rotation around one of the three axes of the Bloch sphere each with probability p/3. The readout error, on the other hand, models the deviations in the measurement output due to various imperfections, such as decoherence, relaxation, or measurement apparatus issues.

To stay consistent between the different schemes and averages, we fix the same logical qubit to device qubit error index mapping, i.e., the qubit layout, ensuring the topology mapping remains a linear geometry. The exact layout used for simulations can be seen in Appendix B. Thus, when the number of qubits is, say, five, the simulation uses only the qubits labeled [0, 1, 2, 3, 4] (in Fig. 17) for a given state transfer scheme. This means that qubit 'zero' is treated as the starting qubit, and qubit 'four' is treated as the end qubit for the state transfer in that case for example.

Fixing that layout, the circuit was then transpiled using the FakeMontreal backend and executed using the QASM simulator with 8192 shots. We ensure that, for all our simulations, we do not rely upon any particular initial state. Indeed, we sample all initial states in all our Qiskit simulations from a random seed and average our results over all the randomly sampled initial states with a large number of shots for each and every scheme—allowing us to reasonably assess the general performance and trend on average.

We found that, overall, the SWAP scheme performed the best, then the cluster scheme (though closely followed by the teleportation scheme) with the GHZ scheme performing the worst as the qubits in the circuit increased. This is evident from Fig. 5, which shows how the numerical value of the expectation value of measuring zero (where, again, zero indicates successful state transfer in our setup) on the final qubit (to which the initial state is being transferred to) changes—for each state transfer scheme—as the number of connected intermediary qubits increases between the starting qubit/site and the end qubit/site.



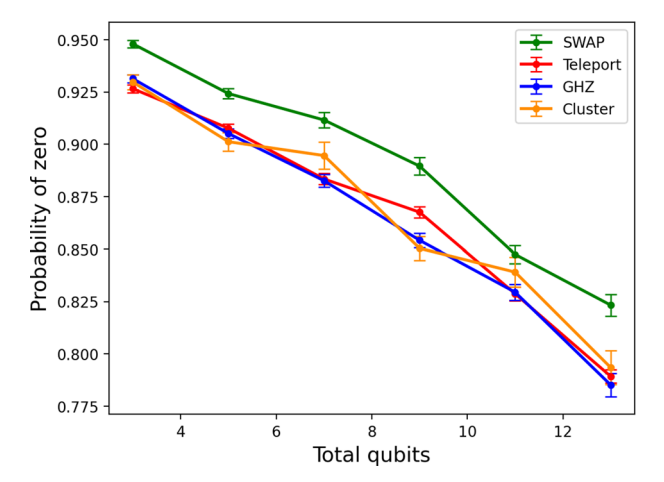


Fig. 5 A plot of the expectation value of zero (where measurement of zero indicates successful state transfer and a measurement of one, failure) varies with increasing qubit number in the different circuit schemes. The simulation used all the gate and readout errors from the device noise model of IBM FakeMontreal with 8192 shots for every data point (and each averaged over fifty random initial states). No optimization or mitigation was applied, and error bars represent the standard error in the average value

The nature of the trend observed with the increasing number of qubits is due to the fact that more intermediary qubits are being used to facilitate the state transfer between the starting qubit and the end qubit (an analog somewhat to an increasing distance between a starting site i and an end site j with increasing repeater nodes). The use of increasing intermediary qubits, naturally, introduces more noise as more noisy gate operations are applied—hence continually decreasing the expectation value from the ideal value of one.

However, something may be slightly surprising at first; the SWAP scheme utilizes the most CNOT operations (which tend to have higher gate error rates compared to single-qubit gates and we ensured the SWAP scheme utilized all three CNOT gates composing a single SWAP gate) when compared to the other three schemes. Moreover, the cluster-state and teleportation schemes both utilize the same number of CNOT gates—smaller than that of the SWAP scheme (if that is the only dominant error of concern)—yet the cluster scheme appears to fair slightly better than the teleportation scheme on average.

Closer inspection, however, suggests that perhaps the measurement errors (or readout errors) of the device dominated, or rather, impacted the noisy simulations more so than initially anticipated. This raises a further, seemingly quite important, question of the balance between the cumulative gate errors and the cumulative readout errors in achieving an effective state transfer scheme in a noisy environment.



275 Page 8 of 36 B. Thotakura, T.-C Wei

3 Interplay of readout and gate errors

3.1 Simulations on the interplay

3.1.1 Turning off readout error

To piece out the relative significance of the errors dominant in the previous section, we consider next the effects of having no readout errors in our noise model, namely having ideal measurements whilst maintaining the device gate error noise. Keeping the same conditions for the simulation as previously (i.e., 8192 shots and averaging over fifty random initial states each time), the simulation results of turning off readout errors can be seen in Fig. 6a, which displays the relationship between the nominal successful state transfer probability (i.e., expectation of measuring zero at the final qubit) vs. the total number of qubits present in the circuit. And perhaps more predictably, we find that the SWAP scheme (the circuit with the most CNOT gates) now performs the worst, with the GHZ and teleportation schemes performing best (almost within error, on average).

3.1.2 Turning off gate error

In contrast to that, we also looked at the effects on the scheme performance when the gate errors were set to zero (that is, ideal gate operations), but with active readout errors present—results obtained, again, from IBM FakeMontreal backend simulator. Utilizing the same topology as in previous simulations and setting any Qiskit optimization to zero, we found, interestingly and, by now expectedly, that the SWAP scheme now performs the best. The teleportation scheme is the next best (though by the end, the cluster scheme is better and teleportation worse) and the GHZ scheme performs the worst, on average, though marginally (see Fig. 6b).

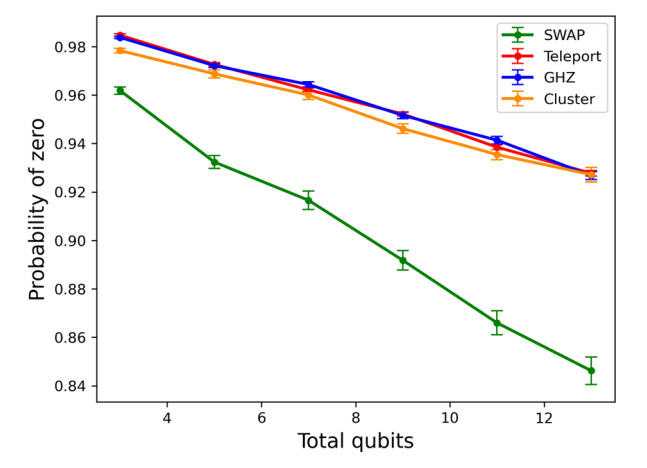
3.1.3 The interplay

To investigate the curious balance and coupled effects of having both a gate error noise model and readout error model on the different state transfer schemes, we consider how the *nominal* success probability varies as a function of varying levels or degrees of gate noise and readout errors. To model such a simulation, we take the gate error model for the circuit basis gates to be a standard depolarizing error model in the Qiskit library (Ref. [47]) controlled by a noise-level parameter p (for $0 \le p \le 1$):

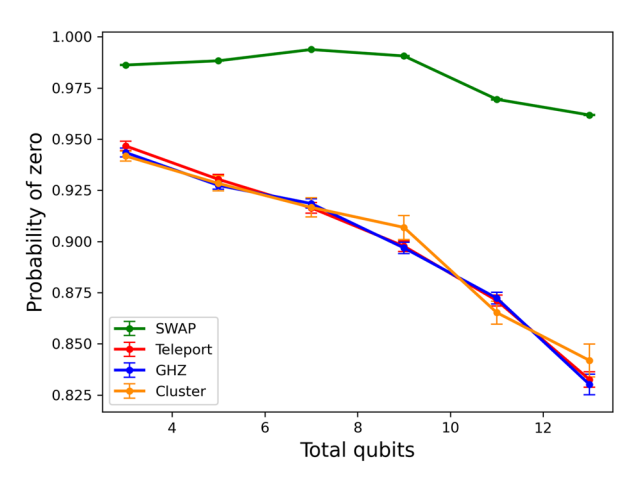
$$\mathcal{E}(\rho) = \left(1 - \frac{4p}{3}\right)\rho + \left(\frac{4p}{3}\operatorname{Tr}(\rho)\right)\frac{I}{2^N} \tag{1}$$

where ρ is the density matrix of the circuit, I is the identity matrix, N the qubit number, and $\text{Tr}(\rho) = 1$ (a normalization we will mostly use). This choice for the gate error model is motivated by Ref. [55] wherein they utilize a depolarizing channel to model the gate infidelities source of error for NISQ devices. Indeed, generally speaking, the depolarization channel is a commonly used gate error for theoretical considerations,





(a) Successful state transfer with device gate noise present only



(b) Successful state transfer with device readout errors present only

Fig. 6 Plots a and b show the variation of the probability of zero when all gate errors and readout errors (in the noise model using IBM FakeMontreal as a backend) are set to zero, respectively. Each data point shown was evaluated with 8192 shots and averaged over fifty randomly sampled initial states at the beginning of the circuit. No circuit optimization or mitigation was applied, and all error bars represent the standard error in the average value

and as discussed in Ref. [56], being able to error-correct the depolarizing channel automatically allows us to error-correct an arbitrary single-qubit quantum operation. Hence, it is an important noise channel to continue to study and use towards such a goal, guided by our understanding of its interplay. Furthermore, from the perspective of simulation, Qiskit's backend noise model utilizes a depolarizing error for both its single- and two-qubit gate errors. Thus, we believe it is appropriate to, by and large, consider for the purposes of our particular study the depolarizing channel. Lastly, we note that for simplicity and our particular analysis (that is, a focus on gate error noise



that does not consider other types of noise such as crosstalk noise for example), we assume uncorrelated error between different qubits. So, for the case of CNOT gate error, we take a tensor product of depolarizing error (similar to Ref. [41]) for analytic and Qiskit numerical simulations.

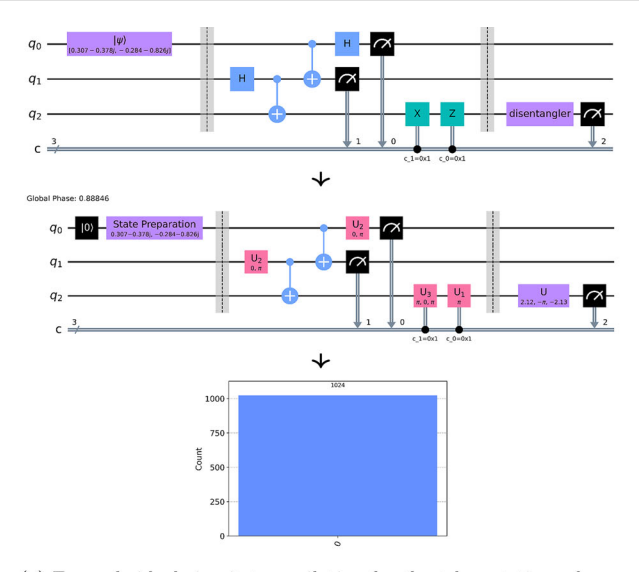
Following the notation of Ref. [47], the readout error is given via the conditional probability P(B|A) which stores the probability of recording a true measurement outcome, A, as instead a misread outcome, B. For our numerical simulations, we take the offset 'symmetric' case where $[P(0|0), P(1|0)] = [1 - P(1|0), P(1|0)] = [1 - \frac{q}{2}, \frac{q}{2}]$ and [P(0|1), P(1|1)] = [P(0|1), 1 - P(0|1)] = [q, 1 - q]. That is, we consider only a single parameter (and in that sense, we loosely say 'symmetric'), q, that controls the probability of recording a true measurement outcome of say one, as zero for example. We note that the factor of $\frac{1}{2}$ is introduced in [P(0|0), P(1|0)] to take into account that $|0\rangle$ is a lower energy state than $|1\rangle$ and hence is more likely to be measured due to decay.

Given this arrangement, we define a custom noise model that is applied to all the standard basis gates in a given quantum circuit and run the simulation to find the probability of measuring zero on the final qubit in the circuit. On the IBM simulator, the gate error model is implemented by having a subset of noisy basis gates (for our simulations, we use U_1 , U_2 , U_3 and CX gates) that contain the particular noise model 'applied'. Then, when a quantum circuit is transpiled with noise, all gates present in the circuit are stripped of their labels and 'unrolled' into a corresponding noisy basis gate. The readout error model is implemented via matrix multiplication, mapping the counts based on a matrix of error probabilities (called the response matrix). This transpilation is illustrated in Fig. 7a, b.

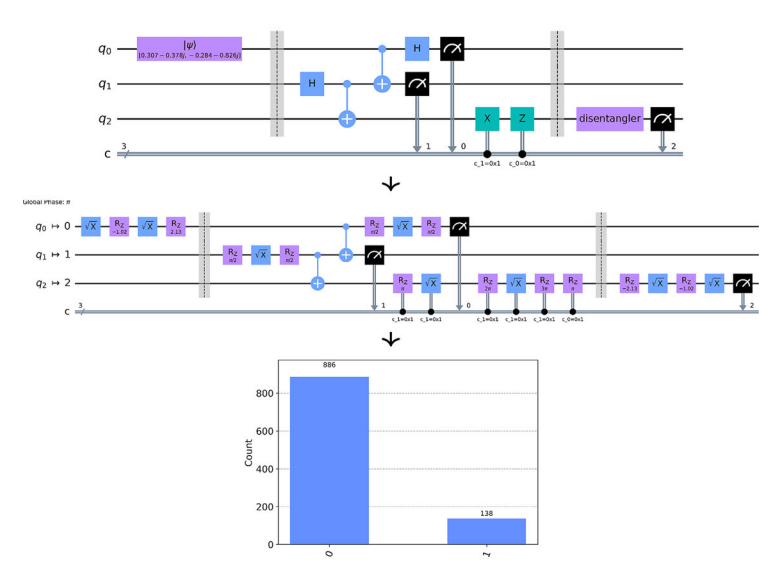
By varying the domain of q and p values input into our custom noise model, we can generate a surface plot of the nominal success probability as a function of q and p. If we take, for example, say, seven qubits in each of our circuit schemes, we yield the surface plots seen in Fig. 8 (with plots of the three- and five-qubit cases in Appendix D). Each of the surface plots is composed of $1600 \ (q, p)$ simulation data points to create the underlying mesh grid. Every single one of those data points used 1024 shots and whose expectation value was averaged over five random initial states (so an effective 5120 shots per data point present). While we may be limited in the number of random initial states we can average over in a finite numerical simulation, we hold that our results give a general indication of a given scheme's performance with scaling errors regardless of the initial state as our random initial state sampling and averaging reasonably suppress any fluctuations on various simulation runs. We are further reassured by the results seen later in Sect. 3.2, where we were able to integrate over the entire Bloch sphere, and our resulting expectation value plots are strongly comparable to the numerical simulation expectation value plots we find here.

Examining Fig. 8, a first glance reveals a somewhat expected behavior of decreasing probability of successful state transfer with increasing depolarizing noise and/or readout error for all of the schemes. Taking a further look, however, there is a peculiar pattern that is persistent throughout all of the surface plots in which the success probability appears to be higher for high p and q values than when p is high and q is low. The pattern appears to remain persistent even when averaged over a couple of random initial states and using a large number of shots. Due to the inherent numerical nature





(a) Example ideal circuit transpilation for the teleportation scheme



(b) Example noisy circuit transpilation for the teleportation scheme

Fig. 7 Illustration of the circuit transpilation for the QASM simulator backend with 1024 shots using the teleportation scheme as an example and a random initial state $((0.30719863 - 0.37807185i)|0\rangle$ – $(0.28356911 + 0.82600196i)|1\rangle$). The histograms show the counts for the final qubit of interest (labeled q_2) only. Figure (a) shows the decomposition of the teleportation circuit into the ideal (noise-free), basis gates of the QASM simulator (standardly consisting of the U_1 , U_2 , U_3 and CX (CNOT gate) in Qiskit's gate library). With no noise model, this transpiled circuit yields the correct expected counts. (b), on the other hand, shows a circuit decomposition into particular noisy basis gates (our custom noise model simulations use the I(identity), CX, R_Z (z-axis rotation gate), \sqrt{X}) gates as the noisy basis gates and a noisy measure operation) from a given noise model (in this case depolarization error model and readout error). This is what we mean by applying a gate and readout error model to a circuit, and we can see that this circuit's counts histogram deviates from the ideal due to the presence of noise



275 Page 12 of 36 B. Thotakura, T.-C Wei

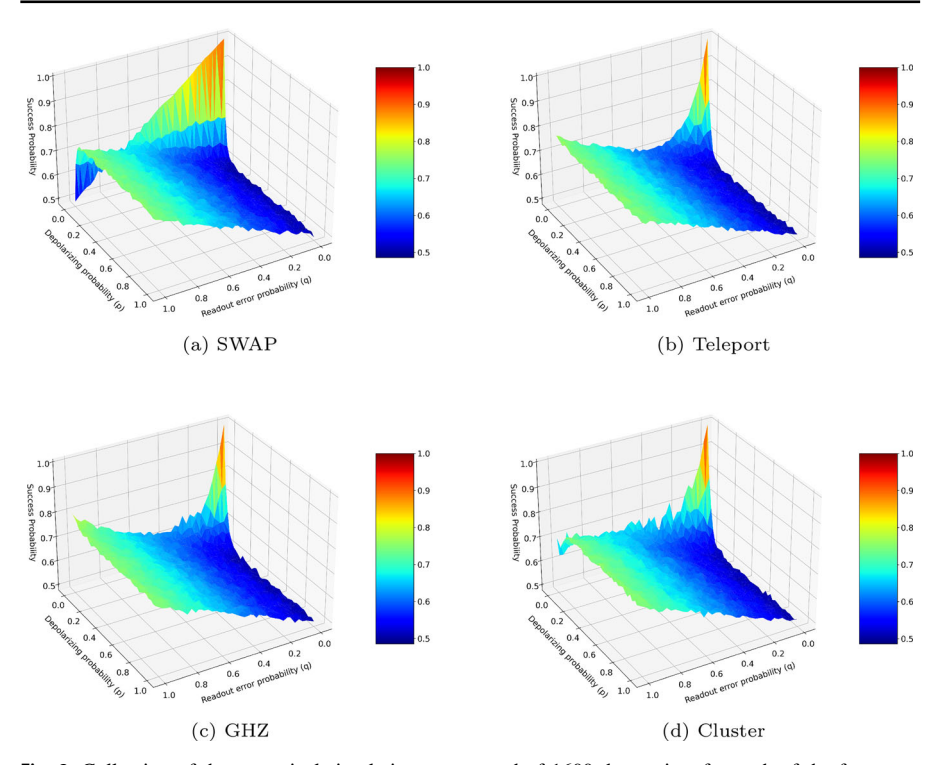


Fig. 8 Collection of the numerical simulations composed of 1600 data points for each of the four state transfer schemes using a seven qubit circuit using 1024 shots (and averaged over five random initial states for every single data point on the surface mesh). The custom noise model used consisted of depolarizing gate error (controlled via parameter p) and a readout error model (characterized via parameter q), with no error mitigation applied. The z-axis of the plots represents the nominal success probability for the particular state transfer scheme. We note that results for three and five qubits are shown in Appendix D

of producing the plot, however, it can be costly (in compute) to generate a sufficiently smooth surface for the success probability to analyze more closely. As an alternative, we sought to take advantage of machine learning surface regression methods from libraries such as scikit-learn SVM (support vector machines); see, e.g., Ref. [57]. For our purposes, scikit-learn SVM has SVR (support vector regression) that would allow us to create a predicted surface regression using the raw numerical data from Fig. 8. This would give us an expected surface that could allow one to predict or interpolate the success probabilities, approximately, for (q, p) data point values not evaluated in the raw numerical simulations of Fig. 8. Such regression surfaces, for each of the state-transfer schemes (visualized with Plotly, see Ref. [58]) with the same seven qubits, can be seen in Fig. 9.

We see that these predicted regression surface plots emphasize the peculiar patterns seen in the standard numerical simulations with the almost exaggerated dip in success probability seen when p is around or less than 0.5 and when q is around or less than 0.2. We also point out that though all these plots show how the nominal success probability of state transfer varies, it can also be closely connected to a meaningful measure of



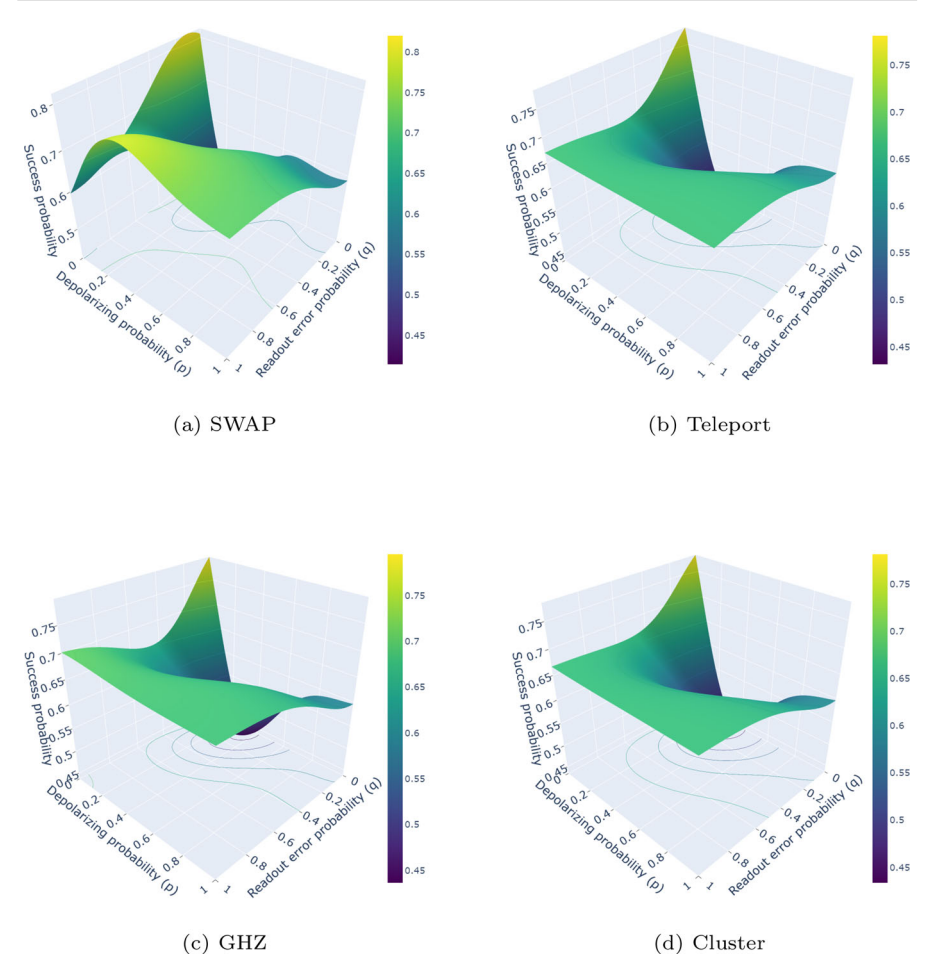


Fig. 9 Smooth SVR (support vector regression) generated surface plots for each of the four schemes on their nominal success probability in state transfer. Similar behavior is present in Fig. 8, with the dip in 'success' probability being more starkly visible at low readout error and moderate levels of depolarizing error

Hellinger fidelity of the state transfer. This arises from the emphasis on the probability distribution, and we are especially led to believe this seeing how the Hellinger fidelity surface plots (see Fig. 20) mirror nominal success surface plots of Fig. 8. This further adds interest to our investigation seeing how the interplay of gate and readout errors impacts fidelity measures.

These results so far implore us to consider more carefully a somewhat counterintuitive interplay between how the quantum error channel and the classical readout error model affect each other. As an aside, we also find similar interplay effects from using an individual Pauli error model instead (see Appendix F), suggesting that this is not necessarily a feature of the depolarizing error model only. To tease out that interplay, we turn towards an analytic understanding of the process in the next subsection. In particular, by observing that our trend of interest is present at all total qubit circuit



275 Page 14 of 36 B. Thotakura, T.-C Wei

lengths—as low as a three-qubit circuit (see Fig. 18 in Appendix D)—it suffices to study and analytically calculate the success probability of state transfer from a three-qubit density matrix to reveal the interplay. Furthermore, we need only consider three of the four outlined schemes as the teleportation and GHZ schemes are equivalent at the three-qubit level of interest.

3.2 Analytical results

To start the analysis, we take an arbitrary initial density matrix, ρ_i , of a three-qubit system (dim(ρ_i) = 8 × 8) to be just:

$$\rho_{i} = |\psi_{i}\rangle\langle\psi_{i}| = \begin{pmatrix} \cos^{2}(\theta/2) & \frac{1}{2}e^{-i\phi}\sin(\theta) & 0 & \cdots & 0\\ \frac{1}{2}e^{i\phi}\sin(\theta) & \sin^{2}(\theta/2) & 0 & \cdots & 0\\ 0 & 0 & \vdots & \ddots & \vdots\\ \vdots & & \vdots & & & \\ 0 & 0 & 0 & \cdots & 0 \end{pmatrix}, \tag{2}$$

where the components along both the row and column are listed in the order of $|000\rangle$, $|100\rangle$, $|010\rangle$, $|111\rangle$, and our initial state is given by the state $|\psi_i\rangle = |\tau_i\rangle|00\rangle$ and our arbitrary state to be transferred given by $|\tau_i\rangle = \cos{(\theta/2)}|0\rangle + e^{i\phi}\sin{(\theta/2)}|1\rangle$. We assume $|\tau_i\rangle$ can be initialized via a gate \mathcal{I} (subject to gate noise) from an initial $|0\rangle$ state by applying the general U-gate,

$$\mathcal{I} = U(\theta, \phi, 0) = \begin{pmatrix} \cos\left(\frac{\theta}{2}\right) & -\sin\left(\frac{\theta}{2}\right) \\ e^{i\phi}\sin\left(\frac{\theta}{2}\right) & e^{i\phi}\cos\left(\frac{\theta}{2}\right) \end{pmatrix},\tag{3}$$

with our 'disentangler' gate modeled as the inverse matrix of (3).

We model our gate error channel, \mathcal{E} , using the standard operator-sum representation of \mathcal{E} (Ref. [56]) with Kraus operators E_i :

$$\mathcal{E}(\rho) = \sum_{i} E_{i} \rho E_{i}^{\dagger}, \tag{4}$$

where our primary Kraus operators used for the depolarizing channel (with probability *p*) are

$$E_0 = \sqrt{1 - p}I, E_1 = \sqrt{\frac{p}{3}}X, E_2 = \sqrt{\frac{p}{3}}Y, E_3 = \sqrt{\frac{p}{3}}Z,$$
 (5)

and if applicable, the following for a bit flip:

$$E_0 = \sqrt{\widetilde{p}}I, E_1 = \sqrt{1 - \widetilde{p}}X, \tag{6}$$

and a phase-flip:



$$E_0 = \sqrt{\widetilde{p}}I, E_1 = \sqrt{1 - \widetilde{p}}Z, \tag{7}$$

channel of probability \widetilde{p} , with I as the identity matrix and X, Y, Z the standard Pauli matrices (see also Appendix F). We consider only a single-qubit version of the depolarizing channel and merely apply a tensor product of the single-qubit depolarizing channel when adding error to two-qubit gates, such as CNOT (similar to our Qiskit numerical simulations).

As brought up, e.g., by Sun, Jinzhao, et al. in Ref. [59], the noise impact for a digital gate-based quantum computer can usually be simplified to a quantum channel appearing either before or after each gate operation. And so, for all error channels, we chose to evolve the density matrix through the error channel after applying the ideal, desired quantum gate operation to model a noisy gate analytically. This kind of modeling, for example, is also used in the discrete event quantum network simulator, NetSquid [60], where they tend to model each noisy operation, $\mathcal{O}_{\text{noisy}}$ as the ideal operation \mathcal{O}_{ideal} followed by a noise channel, \mathcal{N} , such that: $\mathcal{O}_{noisy} = \mathcal{N} \circ \mathcal{O}_{ideal}$. Moreover, this stays in line with the documentation of Qiskit's quantum error class that we used in our numerical simulations, as it states that it describes CPTP (completely positive trace-preserving) gate errors that can be applied after gate or reset instructions, or before measure instructions. Our modeling choice is substantiated further by the fact that Oiskit Aer (the Oiskit module containing the noise model class we used in our numerical simulations) is tailored for Markovian circuit-based noise models. That is, they can always be represented as an ideal operation followed by CPTP maps, as noted by Christopher J. Wood in Qiskit's GitHub repository. This meets our working assumption and hence why, for simplicity, we proceed that way in our analytical considerations as, generally, errors are modeled by adding stochastic errors to the ideal gate operations, while readout errors are modeled by applying a measurement error model to the measurement results.

Next, for the final measurement readout dependent error, we restrict ourselves to the classical single-qubit readout error model [61] (see also Ref. [62]) on the final qubit to which the state $|\tau\rangle$ has been transferred to. Indeed, with our 'disentangler' gate, we are primarily just interested in the measurement outcome '0' ('1') as our criterion for the nominal success of (failure of) state transfer. Thus, we obtain the recorded outcomes, $\widetilde{\mathbf{m_i}} = (\widetilde{m_0}, \widetilde{m_1})^T$, with our single-qubit readout error model by applying the response matrix, Λ , to the true measurement outcomes $\mathbf{m_i} = (\mathrm{Tr}[|0\rangle\langle 0|\rho_f], \mathrm{Tr}[|1\rangle\langle 1|\rho_f])^T \equiv (m_0, m_1)^T$ as follows:

$$\begin{pmatrix} \widetilde{m}_0 \\ \widetilde{m}_1 \end{pmatrix} = \begin{pmatrix} 1 - q_0 & q_1 \\ q_0 & 1 - q_1 \end{pmatrix} \begin{pmatrix} m_0 \\ m_1 \end{pmatrix} \tag{8}$$

where we define q_0 and q_1 to be conditional probabilities P(1|0) and P(0|1), respectively. To restrict the number of free parameters, we take $q_0 = \kappa q$ (for some positive real number κ) and $q_1 = q$ for all proceeding analyses.



There exists a further issue of single-shot readout error that gives rise to the accumulating readout-caused error. Such errors are only of concern in the teleportation, GHZ, and cluster state schemes, wherein intermediate measurement-outcome-dependent errors (or just intermediate readout errors) from the ancillary qubits can lead to accumulating, incorrect application of the correcting measurement-outcome-based conditional gate. Accounting for single-shot readout error is a more difficult problem, and so for our purposes (where we primarily only care about average expectation values), we consider an alternative approximation that could account for such accumulating errors at the qualitative level.

Assuming that the accumulation of such errors occurs with the same probability, $q_0 = \kappa q$ (or $q_1 = q$ depending on random measurement outcome), we attempt to account for such intermediary errors by applying a bit-flip channel (for X measurement conditional gate) and a phase-flip channel (for Z measurement conditional gate). In practice, as an example, this would mean our analytical calculation for the teleportation scheme, after measurement of the first qubit as, say, zero would evolve the density matrix through a phase flip channel of probability $1-q_0$. In other words, the channel would model applying the identity with probability $1-q_0$ (occurs the majority of the time if q_0 is small) and applying a Z gate with probability q_0 . This is because one would normally only need to apply the identity gate as the corrective, measurement-outcome conditional gate if the first qubit measurement outcome is one. But, a readout error model mistaking the true measurement of zero as a one signals that a Z gate needs to be applied before proceeding (incorrectly, from an outside perspective)—and we assume that such incorrect application, in this scenario, occurs with probability q_0 .

Given our setup so far, if we work out (via standard matrix multiplication) the evolution of ρ_i through the three-qubit SWAP scheme unitaries, whilst individually applying a tensor product of the single-qubit depolarizing error channel (same as done in our custom noise model in the Qiskit simulations) after every CNOT gate operation, one finds the following normalized, *average* (integrated) expected measurement outcomes, \bar{m}_i , for the final qubit, as a function of the depolarizing parameter p:

$$\bar{m}_{0,\text{swap}}(p) = 1 + \sum_{j=1}^{12} \frac{(-1)^j [\mathbf{A}_{\text{swap}}]_j 2^{(2j-1)}}{3^{(j+1)}} p^j$$
(9)

where $\mathbf{A}_{\text{swap}} = (32, 156, 460, 915, 1296, 1344, 1032, 585, 240, 68, 12, 1)^T$. We note that integration over the entire Bloch sphere is performed to obtain all true average measurement outcomes in this subsection as follows:

$$\bar{m}_i = \frac{1}{4\pi} \int_0^{2\pi} \int_0^{\pi} \text{Tr}[|i\rangle\langle i|\rho_f(\theta,\phi)] \sin\theta \, d\theta \, d\phi. \tag{10}$$

Applying our final measurement readout error model, and using the fact that $1-\bar{m}_{0,(\text{scheme})} = \bar{m}_{1,(\text{scheme})}$, we get that the nominal success probability for state transfer, that is, \tilde{m}_0 , is given by:

$$\widetilde{m}_0(q, p) = q + \overline{m}_0(1 - (\kappa + 1)q).$$
 (11)



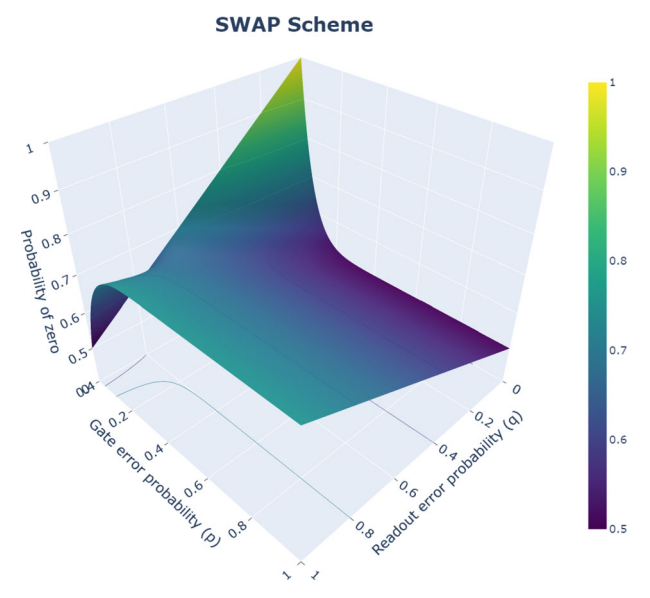


Fig. 10 Nominal success probability surface plot of Eq. (11) (after input of Eq. (9)) for the SWAP scheme circuit with three qubits

Plotting Eq. (11) using the function from Eq. (9) for, like our previously chosen, $\kappa = \frac{1}{2}$ (see Fig. 10), we begin seeing the trends observed in the previous numerical Qiskit simulations exactly. That is, for the SWAP scheme, we evidently see the same structure with the same linear drop-off near the p=0 plane and a dip in the expectation value near low readout error and high gate error that was peculiar to us before.

Accordingly, following similar calculations, but now for the teleportation and cluster-state schemes (using the same depolarizing channel but accounting for the possible accumulating intermediary readout error, q, with either bit or phase flip channels), we find the following for the three-qubit teleportation (from which we can safely infer the three-qubit GHZ circuit scheme as well) and cluster-state schemes,

$$\widetilde{m}_{0,\text{(scheme)}} = q + (1 - (\kappa + 1)q) \sum_{n=0}^{10} \sum_{k=0}^{2} [\mathbf{A}_{\text{(scheme)}}]_{nk} \frac{(-1)^{(n+k)} 2^{(2n-k-1)}}{3^{(n-k+1)}} q^k p^n,$$
(12)

with, respectively,

$$(\mathbf{A}_{\text{teleport}})^T = \begin{pmatrix} 6 & 26 & 102 & 239 & 371 & 399 & 301 & 157 & 54 & 11 & 1\\ 4 & 36 & 147 & 359 & 581 & 651 & 511 & 277 & 99 & 21 & 2\\ 1 & 10 & 45 & 120 & 210 & 252 & 210 & 120 & 45 & 10 & 1 \end{pmatrix},$$
 (13)



275 Page 18 of 36 B. Thotakura, T.-C Wei

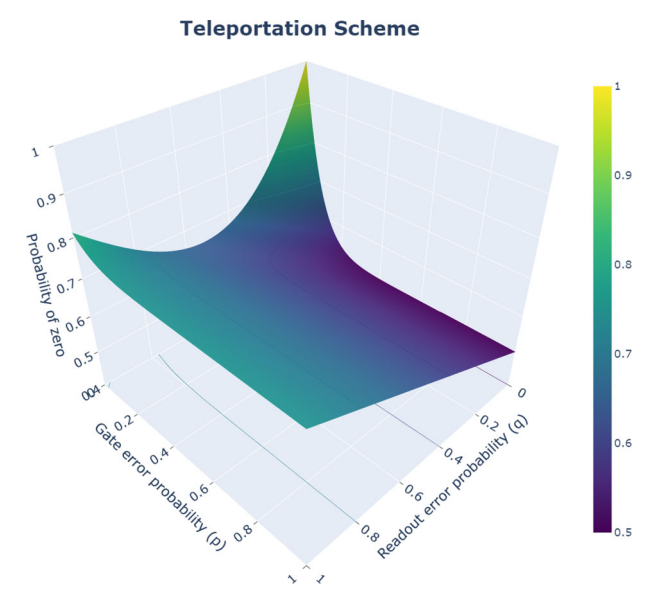


Fig. 11 Nominal success probability surface plot of Eq. (12), using the coefficients from (13) for the teleportation scheme with three qubits. The plot gives insight into a three-qubit GHZ scheme as well due to the circuit equivalence at the three-qubit level

and

$$(\mathbf{A}_{\text{cluster}})^T = \begin{pmatrix} 6 & 26 & 105 & 260 & 435 & 510 & 421 & 240 & 90 & 20 & 2 \\ 4 & 40 & 180 & 480 & 840 & 1008 & 840 & 480 & 180 & 40 & 4 \\ 2 & 20 & 90 & 240 & 420 & 504 & 420 & 240 & 90 & 20 & 2 \end{pmatrix}.$$
 (14)

We note that \bar{m}_0 for the cluster and teleportation is an average of the four possible measurement outcomes of the ancilla qubits. The plots of Eq. (12) with coefficients from (13) and (14) can be seen in Figs. 11 and 12, respectively (with $\kappa = \frac{1}{2}$ as before).

With our sole analytic analysis, we can now explain (and replicate) the peculiar behavior of low readout error and high gate noise resulting in the lowest successful state transfer with our analytic expressions. Indeed, from these results, we can glean that at high readout error and high gate noise, there is so much classical readout flipping of the true measurement result that it seems to 'counteract' the decrease in the measurement of the zero outcomes from the gate noise. Furthermore, the asymmetry in the readout error model appears to be creating a 'biasing' effect where the recorded measurements of particular outcomes become more common at certain levels of readout error that it appears to give better results at the nominal success level. This suggests that there can exist 'minima' at each readout error and gate noise produces the lowest nominal success rate, and that higher values can have some sort of 'interference' effect of counteracting each other. Grasping this concept can perhaps lead to using particular levels of readout error to one's advantage and/or applying error mitigation techniques more effectively to 'steer' where pockets (of minima) of lowest, nominal success probability can appear. As a further possibility, it could allow one to better avoid



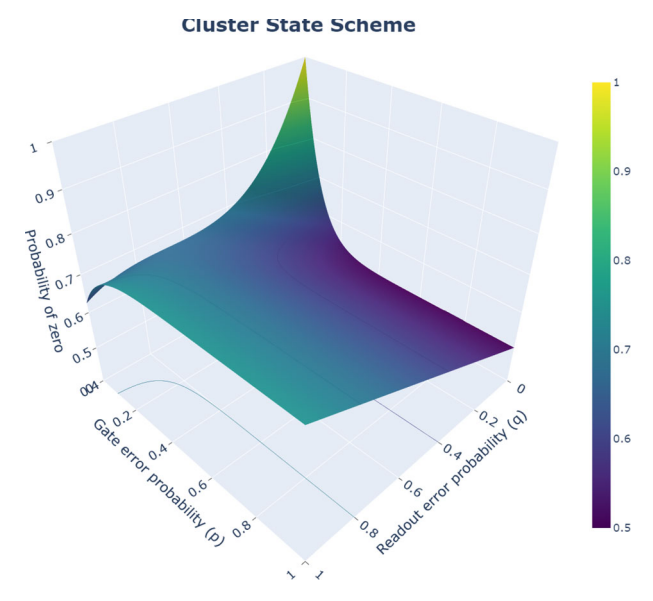


Fig. 12 Nominal success probability surface plot of Eq. (12) (using the specific input of (14)) for the cluster state scheme with three qubits

minima pitfalls if performing noise-scaled regressions and building noise-learning models.

On the flip side, one could also ask if there are any similarities of such trends in the actual state fidelity as well—or even how exactly the functional form and coefficients change in contrast. While we cannot output the exact state vector of a qubit state on a real device, our analytic methods allow us to work out the fidelity by omitting the final 'disentangler' gate unitary and final qubit measurement. Computing the density matrix evolution exactly as before, we can then compute the average state fidelity, F, as a function of the noise parameters p and q (where, again, q is now a stand-in for any incorrect application of intermediary measurement dependent gate due to incorrect readout of ancilla qubits) with the commonly used formula (Ref. [63, 64]):

$$F(q, p) = \frac{1}{4\pi} \int \langle \tau | \rho | \tau \rangle d\Omega, \qquad (15)$$

where the integration is over the entire Bloch sphere again, and $|\tau\rangle$ is an arbitrary initial state.

For the SWAP scheme, which has no measurement-dependent gates, we get the average fidelity (referred to as just the fidelity in the plots and text henceforth for brevity) as purely a function of p:

$$F_{\text{swap}}(p) = 1 + \sum_{j=1}^{11} \frac{(-1)^j [\mathbf{B}_{\text{swap}}]_j 2^{(2j-1)}}{3^{(j+1)}} p^j$$
 (16)



275 Page 20 of 36 B. Thotakura, T.-C Wei

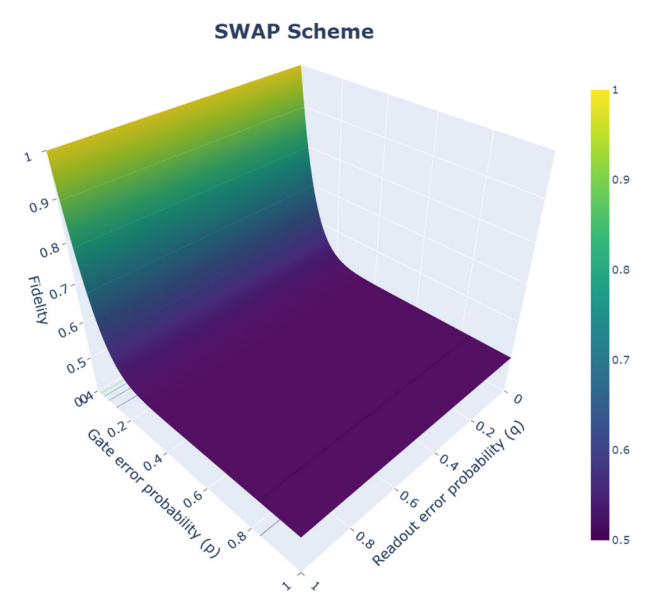


Fig. 13 Final state fidelity surface plot from a three-qubit SWAP scheme with varying depolarizing noise, p, and no intermediary readout error q dependence, following Eq. (16)

where $\mathbf{B}_{\text{swap}} = (29, 127, 333, 582, 714, 630, 402, 183, 57, 11, 1)^T$. For the teleportation and cluster-state schemes, the fidelity functions are now both a function of p and recontextualized q, and they are given by:

$$F_{\text{(scheme)}} = \sum_{n=0}^{9} \sum_{k=0}^{2} [\mathbf{B}_{\text{(scheme)}}]_{nk} \frac{(-1)^{(n+k)} 2^{(2n-k-1)}}{3^{(n-k+1)}} q^k p^n$$
 (17)

with, respectively,

$$(\mathbf{B}_{\text{teleport}})^T = \begin{pmatrix} 6 & 23 & 79 & 160 & 211 & 188 & 113 & 44 & 10 & 1 \\ 4 & 32 & 115 & 244 & 337 & 314 & 197 & 80 & 19 & 2 \\ 1 & 9 & 36 & 84 & 126 & 126 & 84 & 36 & 9 & 1 \end{pmatrix}$$
 (18)

and,

$$(\mathbf{B}_{\text{cluster}})^T = \begin{pmatrix} 6 & 23 & 82 & 178 & 257 & 253 & 168 & 72 & 18 & 2 \\ 4 & 36 & 144 & 336 & 504 & 504 & 336 & 144 & 36 & 4 \\ 2 & 18 & 72 & 168 & 252 & 252 & 168 & 72 & 18 & 2 \end{pmatrix}$$
 (19)

with the respective plots of the fidelity functions shown in Figs. (13, 14 and 15).

Looking at those fidelity plots, we notice that the stark dip observed previously is not quite expressly present at the low readout and high depolarization noise. Though, there is some resemblance to the contours of the success probability surface plots of



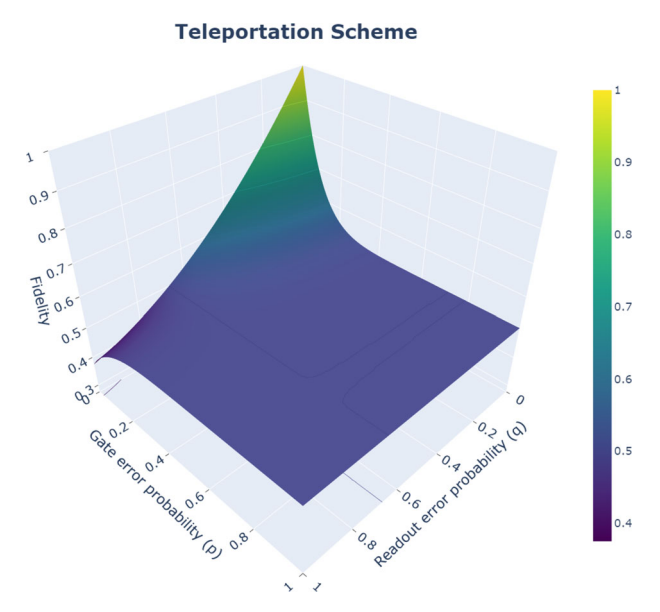


Fig. 14 Final state fidelity surface plot from a three-qubit teleportation scheme with varying depolarizing noise (p) and intermediary readout dependent error, q, following Eq. (17) and the coefficients of (18)

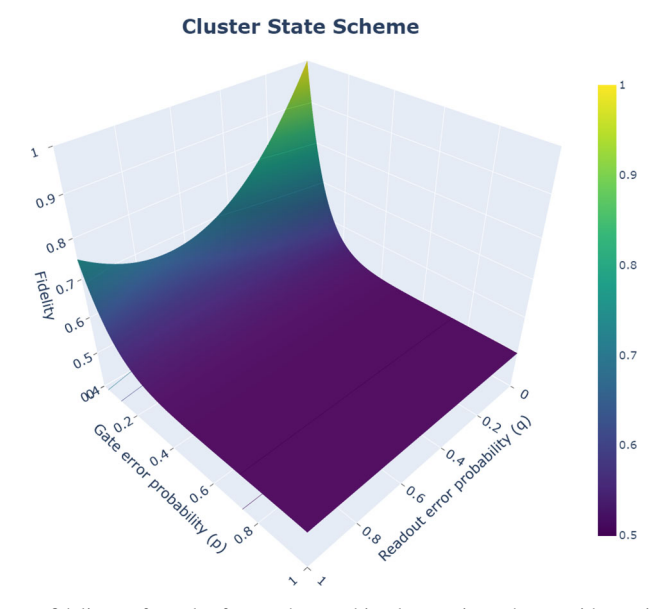


Fig. 15 Final state fidelity surface plot from a three-qubit teleportation scheme with varying depolarizing noise, p, and intermediary readout dependent error, q, following Eq. (17) and the coefficients of (19)



Figs. 10, 11 and 12 near the small gate error region, the high noise and high readout behavior in the fidelity surface plot is different because the surface tends to decrease and plateau. Still, the functional form of the fidelity matches closes with our measure of the success probability, differing most significantly in the particular coefficients of $A_{\rm (scheme)}$ and $B_{\rm (scheme)}$. This is illuminating in how different fidelity measures differ and also highlights an important note: how the measured nominal 'counts' from a real device, from a black box lens, may differ significantly in behavior to analyzing the state fidelity. These results showcase what the role readout and gate error play in biasing that expectation value—and the almost non-monotonic relationship they have to the nominal expectation value.

4 Error mitigation possibilities

With our understanding of the role of gate and readout errors, a natural question to ask would be if we could leverage our analysis so far to mitigate errors. Given that throughout the paper we only accounted for gate errors, a technique such as zero-noise extrapolation ([45, 46]), or ZNE for short, can be a powerful tool to mitigate noisy (from real device noise models) expectation values. The question of mitigating accumulated measurement outcome-dependent errors (call it intermediate readout resultant errors) can be more tricky. In the case of the SWAP scheme, merely inverting the response matrix, Λ , in Eq. (8) would be sufficient — as there are no measurement-outcome-based conditional gates. Unfortunately, mitigating the accumulated readout-caused errors for the other schemes is not as straightforward as that requires shot-by-shot mitigation. However, given that we are particularly dealing with mitigating average expectation values, we could attempt to apply an approximate inverse response matrix, Λ^{-1} , and assess how well it can mitigate accumulated readout error on average. One possible way to go about mitigating real device noise could be to compare ZNE mitigated expectation values ('probability of zero' or 'successful counts' depending on the context) and extrapolate the amount of accumulated readout error, on average, was needed to achieve that particular ZNE mitigated expectation value from the surface plots we have generated (on the contour of p = 0).

With that idea in mind, a plot of how the expectation value of zero, E, degrades with increasing partial gate set, G, folding can be seen in Fig. 16 for a three-qubit circuit. We chose to implement the gate folding following scheme outlined in Ref. [45], wherein our circuit depth, of say D, is scaled to αD after gate folding. For our circuits, we folded the Hadamard (H) and CNOT subset of gates and kept all else the same. From there, following Ref. [45] again, we extrapolate to the zero-noise limit of $E(\alpha = 0)$ (as can be seen via the vertical, dashed black line in Fig. 16) by performing an exponential fit of the form $E(\alpha) \sim ae^{-b\alpha} + c$. An example dataset of the three-qubit ZNE mitigated expectation values for a particular random initial state can be seen in Table 1.

Next, to attempt to mitigate the accumulated readout-caused error, we apply Λ^{-1} (keeping $q_0 = \frac{q}{2}$ and $q_1 = q$) to the ZNE mitigated values. To get a good estimate for the average q in Λ^{-1} , we extrapolate its value, for a given scheme, from the respective



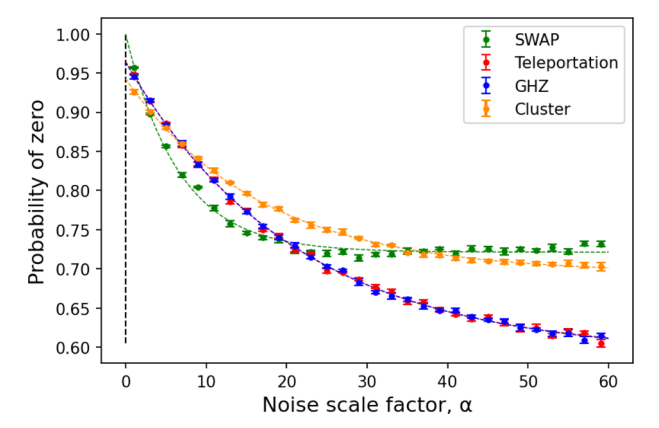


Fig. 16 Three-qubit circuit scheme expectation values, E, for measuring zero (i.e., the probability of zero) with increasing noise scaling parameter, α (controlling the CNOT and H gate folding in the circuits), to interpolate the zero noise limit of $E(\alpha = 0)$. The noise model used for the data points is from IBM FakeMontreal, with each data point having 4098 shots and each expectation value averaged five times (with error bars representing the standard error in that average). The initial state vector sampled for this specific data is $|\tau_i\rangle = (0.79114257 + 0.37436334i)|0\rangle + (0.40615923 + 0.26264083i)|1\rangle$

Table 1 Example dataset of expectation values of zero

Circuit scheme	Unmitigated value	ZNE Mitigated value	Readout mitigated value
SWAP	0.95583	0.99952 ± 0.01250	1.00000 ± 0.01250
Teleportation	0.94436	0.96469 ± 0.00501	0.97728 ± 0.00501
GHZ	0.94802	0.96361 ± 0.00325	0.97662 ± 0.00325
Cluster state	0.92533	0.94260 ± 0.00301	0.96427 ± 0.00301

The unmitigated values are the exact output of the probability of zero for a three-qubit circuit simulation (4098 shots) using IMBQ's FakeMontreal backend noise. The ZNE mitigated values are obtained from doing the extrapolation in Fig. 16. The final column shows the average readout mitigated values from inverting an approximate response matrix A. The initial state vector sampled for this specific dataset is $|\tau_i\rangle = (0.79114257 + 0.37436334i)|0\rangle + (0.40615923 + 0.26264083i)|1\rangle$

scheme's expectation value of zero surface plot. In particular, we would determine the q value present at the point where p = 0 and the z coordinate = the unmitigated expectation value. At the three-qubit level, we can straightforwardly use our analytic equations to determine such a q value for Λ^{-1} . An example of the mitigation possible by this method, for a three-qubit circuit, can be seen in Table 1.

For larger qubit circuits, where specific analytic expressions may be harder to find, one could generate surface plots akin to Fig. 8, but with the axis of increasing gate noise replaced, instead, with increasing ZNE noise parameter, α , from normal device noise. The readout error axis would need to be varied as well, in some probabilistic fashion or by simply updating the device noise model each time. With sufficient data points from many randomized circuits, one could use regression methods (like those used in Fig. 9) to generate a smooth surface plot of the expectation value varying with increasing device noise (α) and readout error. This could allow one to extrapolate q



numerically, for a given expectation value, at the $\alpha = 0$ limit without any analytic expression.

Finally, looking at Table 1, we see that the ZNE mitigation works well to improve the expectation values closer to their ideal (and more so when gate noise is dominant like in the SWAP scheme), and applying an approximate inverse response matrix allows us to mitigate all noise from the SWAP scheme in particular (within some small error margin). While the same is not exactly true for the other remaining schemes, we can still report that the method of surface q extrapolation can at least provide a noticeable improvement in the expectation values for all the three-qubit circuit schemes. This suggests that an approximate response matrix can still have a role in mitigating accumulated readout-caused errors, even if further mitigation techniques would still be required depending on the particular scheme.

5 Conclusion and discussion

In this work, we looked at quantum state transfer at the level of algorithmic protocols to facilitate quantum state transfer. Our results indicate how different state transfer schemes (a successive standard SWAP, standard teleportation, GHZ resource, and cluster state resource) fair in quantum state transfer, from a site i to site j in a linear chain geometry, under the particular gate and readout errors model. We show the unexpectedly significant role readout error can play in choosing a state transfer scheme and primarily illustrate the counterintuitive interplay readout error has with gate noise in measuring nominal expectation values. We also presented analytical equations, for the three-qubit level, that can reproduce and explain that counterintuitive interplay that one sees, through a black-box lens, on a real device. Lastly, we briefly touched upon how error mitigation may enter this picture in helping to determine better scheme performance.

The schemes we worked with can be translated to other schemes involving, for example, those of a SWAP chain state transfer, schemes with time-dependent Hamiltonian applied to a series of qubits to perform state transfer like adiabatic transfer, or gate teleportation in the MBQC framework. It also naturally leads to the advantages of the schemes we presented, which can reduce the overhead effect of gate noise with their native gate connectivity. The SWAP scheme is particularly relevant when a SWAP chain can be utilized between neighboring qubits without the added overhead of intermediary SWAP operations. The teleportation scheme presents advantages between distant qubits that require routing the quantum state where reasonably low readout error overcomes the accumulating error from additional, possibly unnecessary CNOT gates between intermediary qubits. The GHZ scheme may be an alternative if a high-fidelity resource GHZ state is readily available for use and the measurement errors are much less than the gate errors for the system. The cluster state scheme would be particularly advantageous if one was interested in quantum state transfer within an existing lattice cluster state structure or general graph state quantum network. It would also be the preferred way of quantum state transfer in the MBQC framework.

While we only considered gate errors and classical readout errors, there are possible extensions in investigating other noise interconnections than that of just depolarizing noise. Furthermore, one could also extend this work to consider quantum state transfer



in different network geometries and how that changes the scheme performances. Lastly, one could also investigate more sophisticated error mitigation and correction schemes that can perhaps exploit the interplay we have seen in this paper.

Acknowledgements We thank Eden Figueroa and C. R. Ramakrishnan for useful discussions. This work was supported by the National Science Foundation under Grants No. FET-2106447 and No. PHY-1915165. In particular, the research on quantum state transfer was supported by FET-2106447, and the research on the effect of noise and errors and their mitigation was supported by PHY-1915165. We also acknowledge partial support from the Provost's Office of Stony Brook University via a Provost Venture Fund Seed Grant.

Data Availability The datasets generated during and/or analyzed during the current study are available from the corresponding author on reasonable request.

Declarations

Conflict of interest The authors have no competing interests to declare that are relevant to the content of this article.

Appendix A Terminology

Term	Definition		
SWAP	A shorthand for the action of a SWAP gate; a gate which exchanges the states of two qubits. In other words, performs the following map on a two-qubit state: $ \psi\rangle\otimes \phi\rangle\rightarrow \phi\rangle\otimes \psi\rangle$.		
Teleportation	A shorthand for the teleportation protocol which allows one to transfer the quantum state of one qubit to another as independently copying the exact same quantum state onto another qubit is prohibited by the no-cloning theorem. [56].		
GHZ State	An abbreviation for the Greenberger–Horne–Zeilinger state. It is a multi-qubit entangled state with equal superposition of the zero and one states. That is, for N qubits, of the form: $\frac{1}{\sqrt{2}}(0\rangle \otimes N + 1\rangle \otimes N)$.		
Cluster State	An entangled state following a lattice structure wherein each qubit, initialized as $ +\rangle = \frac{1}{\sqrt{2}}(0\rangle + 1\rangle)$ via a Hadamard gate, is connected to its nearest neighbor		
Noise model	via a controlled $Z(CZ)$ gate operation A model of operations that simulates the effects of noise and errors on an input state quantum system to a resulting output quantum state affected by the noise		
Topology mapping	The stage in the quantum circuit transpilation that maps the logical qubits used at the quantum circuit level to physical connectivity (access) of physical qubits on a real device/quantum processor.		
Transmon qubit	A physical qubit can be thought of as a two-level quantum system, and the transmon [65] qubit is a type of superconducting qubit akin to that of an LC oscillator but with the inductor and capacitor analogs being a Josephson junction and capacitance, respectively. The various levels of the superconducting system are isolated to two energy levels to get an approximate qubit.		

Appendix B Device connectivity

We show in Fig. 17 the layout of IBM Q Montreal whose device noise model was used in our simulations. The numbers marked in the diagram show the linear chain that we used in comparing different state transfer schemes.



275 Page 26 of 36 B. Thotakura, T.-C Wei

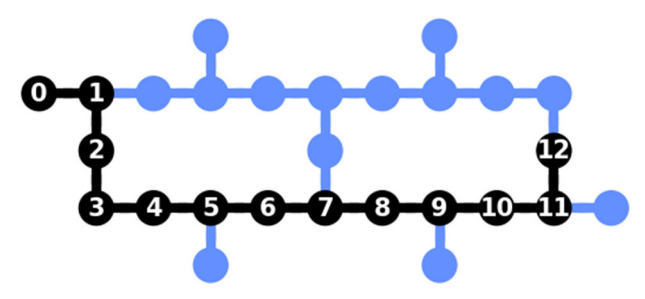


Fig. 17 Linear chain layout of IBM Q Montreal used for all simulations. Specifically, the custom qubit mapping to device qubit mapping is given by [0, 1, 2, 3, 4, 5, 6, 7, 8, 9, 10, 11, 12] = [0, 1, 2, 3, 5, 8, 11, 14, 16, 19, 22, 25, 24], with the latter being the physical qubit labeling on the real device

Appendix C GHZ and cluster schemes

Here we detail the state transfer scheme algorithm given an *N*-qubit circuit at the state level for the GHZ and Cluster state scheme.

GHZ scheme: Suppose that the first qubit of an *N*-qubit (we take $N \ge 4$ and N = 3 as equivalent to the teleportation scheme) system, $|\psi_0\rangle$, is initialized in the normalized state $|\tau\rangle = \alpha |0\rangle + \beta |1\rangle$ and the remaining qubits form a GHZ state like so:

$$|\psi_0\rangle = |\tau\rangle \otimes \frac{1}{\sqrt{2}} \left(|0\rangle^{\otimes (N-1)} + |1\rangle^{\otimes (N-1)} \right)$$
 (C1)

with logical qubit labeling starting from q_0 to q_{N-1} . Applying a CNOT gate between the first (q_0) and second qubit (q_1) then gives,

$$|\psi_1\rangle = \frac{1}{\sqrt{2}} \left(\alpha |00\rangle |0\rangle^{\otimes (N-2)} + \alpha |01\rangle |1\rangle^{\otimes (N-2)} + \beta |11\rangle |0\rangle^{\otimes (N-2)} + \beta |10\rangle |1\rangle^{\otimes (N-2)} \right)$$
(C2)

and after measuring the second qubit in the Z-basis, with measurement outcome $m_1 \in \{0, 1\}$ for q_1 , the state becomes:

$$|\psi_{2}\rangle = \left(\alpha |0m_{1}\rangle \left(\bigotimes_{i=2}^{N-1} X_{i}^{m_{1}}\right) |0\rangle^{\otimes(N-2)} + \beta |1m_{1}\rangle \left(\bigotimes_{i=2}^{N-1} X_{i}^{m_{1}}\right) |1\rangle^{\otimes(N-2)}\right).$$
 (C3)

We then apply a H gate to the first qubit and notice that we can undo the possible byproduct X_i gates (applied to logical qubit q_i) on all the remaining (N-2) qubits by applying measurement-conditional gates, $\bigotimes_{i=2}^{N-1} X_i^{m_1}$ (as $X^2 = I$), to all the qubits aside from the first two so that,

$$|\psi_3\rangle = \left(\alpha |+m_1\rangle |0\rangle^{\otimes (N-2)} + \beta |-m_1\rangle |1\rangle^{\otimes (N-2)}\right),\tag{C4}$$



where the shorthand $|\pm\rangle = \frac{1}{\sqrt{2}}(|0\rangle \pm |1\rangle)$ is used. If we now measure the first qubit in the Z-basis with measurement outcome, m_0 , the resulting state becomes:

$$|\psi_4\rangle = |m_0 m_1\rangle \otimes \left(\alpha |0\rangle^{\otimes (N-2)} + \beta (Z_2^{m_0} |1\rangle) |1\rangle^{\otimes (N-3)}\right). \tag{C5}$$

The possible minus sign on the third qubit can be avoided with a measurement-conditional Z gate. If we continue to apply a H gate to the third qubit like so,

$$|\psi_5\rangle = |m_0 m_1\rangle \otimes \left(\alpha |+\rangle |0\rangle^{\otimes (N-3)} + \beta |-\rangle |1\rangle^{\otimes (N-3)}\right).$$
 (C6)

and measure the third qubit in the computational basis, we will end up in a similar situation as C5 with the remaining state $(\alpha|0\rangle^{\otimes(N-3)}+\beta(Z_3^{m_2}|1\rangle)|1\rangle^{\otimes(N-4)})$, wherein applying a local Z gate, based on the measurement outcome, will correct for the possible minus sign. Lastly, repeating the process for all but the last qubit by applying an H gate, Z-basis measurement on the remaining qubits (with outcome m_i for logical qubit q_i), and a Z correction gate on the respective proceeding qubit yields, by the end, the following state:

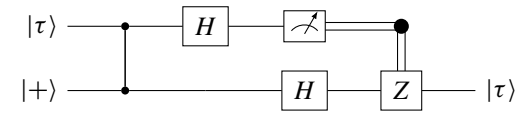
$$|\psi_6\rangle = \left(\bigotimes_{i=0}^{N-2} |m_i\rangle\right) \otimes \left(\alpha |0\rangle + \beta |1\rangle\right) = \left(\bigotimes_{i=0}^{N-2} |m_i\rangle\right) \otimes |\tau\rangle \tag{C7}$$

showing that our initial state, $|\tau\rangle$, has been successfully transferred to the final qubit starting with an initial resource (N-1) qubit GHZ state.

Cluster scheme: To understand the Cluster state scheme, it is illuminating to simply start with the gate teleportation protocol that is used in measurement-based quantum computation (MBQC) from Ref. [66]:

$$R_Z | au
angle \longrightarrow H$$
 m_0 m_0

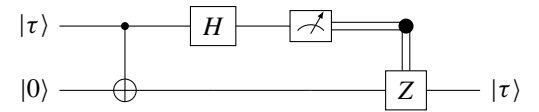
where the gate $U = X^{m_0}HR_Z$ has been teleported given a measurement outcome, $m_0 \in \{0, 1\}$, on the first qubit - which begins in the normalized state $|\tau\rangle = \alpha |0\rangle + \beta |1\rangle$ and an R_Z gate (Z-rotation gate parameterized by some angle θ) operation. We can cancel a possible X^{m_0} gate application via a measurement-conditional X gate. Then, w.l.o.g., we can take R_Z to be an identity gate (by setting its angle parameter to zero). We are then only left with a teleported Hadamard gate, but given our state transfer purpose of obtaining just $|\tau\rangle$, we can exploit the identity HZ = XH to work with:





275 Page 28 of 36 B. Thotakura, T.-C Wei

Thus, we can perform an N-qubit state transfer given an initial (N-1) qubit resource cluster state via several concatenated gate teleportation circuit blocks to form the Cluster state scheme. However, in our simulations, we use CNOT as our basis gate, and so as to not introduce additional gates to convert to CZ gates, we instead work with the following translated circuit instead for all our simulations:



utilizing the identity CNOT = $(I \otimes H)CZ(I \otimes H)$ (see Ref. [54]), given the Hadamard from the initial $|+\rangle$ state and 'teleported' H from before.

Appendix D Success probability for 3 and 5 qubit circuits

In Fig. 8, we show the success probability of different state transfer schemes using seven-qubit circuits; in Figs. 18 and 19, we show the corresponding results with three and five qubits, respectively.

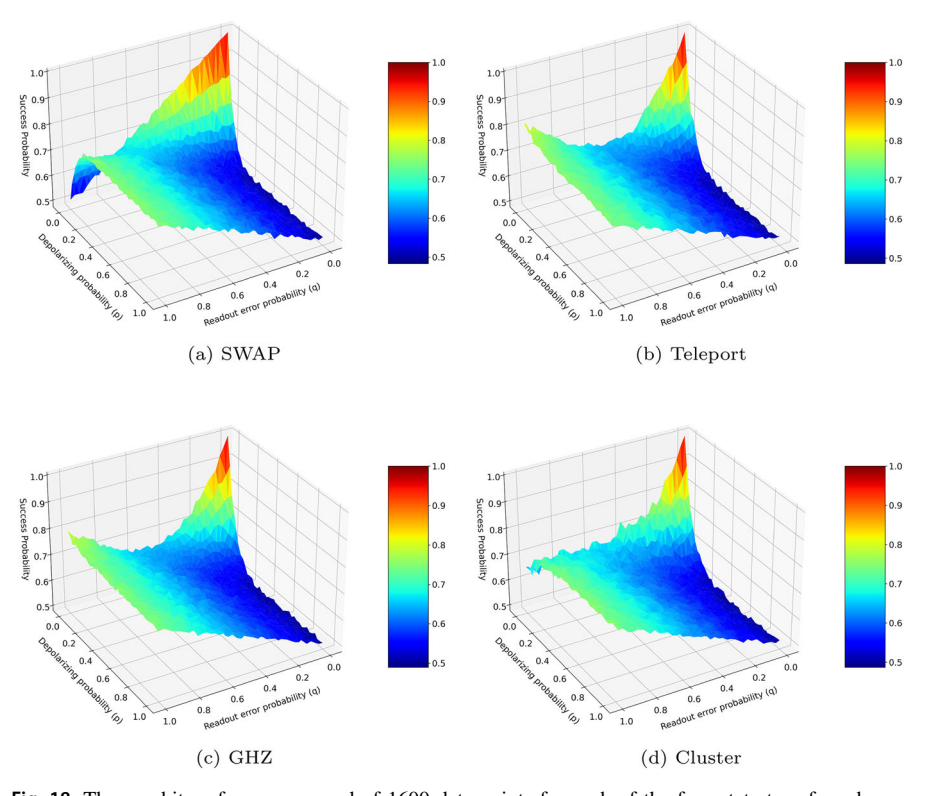


Fig. 18 Three-qubit surfaces composed of 1600 data points for each of the four state transfer schemes using 1024 shots (and averaged over five random initial states for every single data point on the surface). The custom noise model used consisted of depolarizing gate error (controlled via parameter p) and a readout error model (characterized via parameter q), with no error mitigation applied. The z-axis of the plots represents the nominal success probability for the particular scheme of state transfer



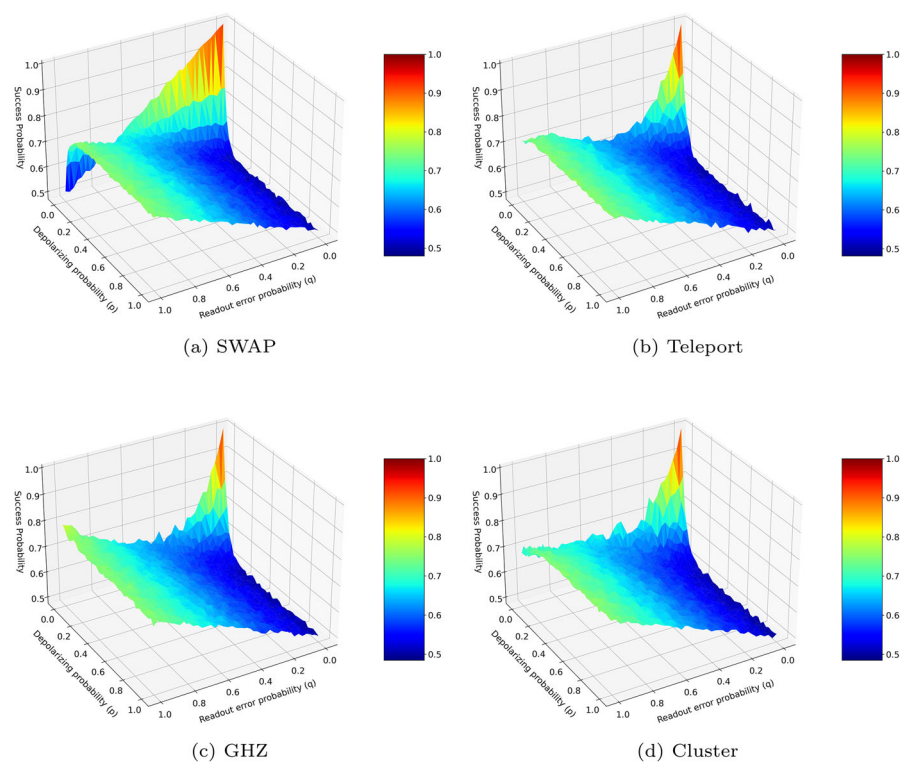


Fig. 19 Five-qubit surfaces composed of 1600 data points for each of the four state transfer schemes using 1024 shots (and averaged over five random initial states for every single data point on the surface). The custom noise model used consisted of depolarizing gate error (controlled via parameter p) and a readout error model (characterized via parameter q), with no error mitigation applied. The z-axis of the plots represents the nominal success probability for the particular scheme of state transfer

Appendix E Hellinger fidelity plots for a 7 qubit scheme

As an aside, we could try to consider another measure for 'successful' state transfer in Qiskit such as the so-called Hellinger fidelity, F_H , [47] defined as:

$$F_H = \left(1 - h^2\right)^2 \tag{E1}$$

where h is the Hellinger distance. This distance h generally tells you the 'closeness' of two probability distributions (in our case, 'counts' distribution) given some observations (see Ref. [67] for more details). We note that this F_H quantity reduces to the quantum state fidelity for diagonal density matrices (i.e., the classical fidelity) [47].

In Fig. 20, we plot how F_H varies with q and p for an example five-qubit case, and interestingly, the surface shapes match closely the structure we saw in Fig. 8. Thus, we see that while our expectation value of zero as the standard for 'successful state transfer' may not be directly related to the exact quantum state fidelity itself, it is



275 Page 30 of 36 B. Thotakura, T.-C Wei

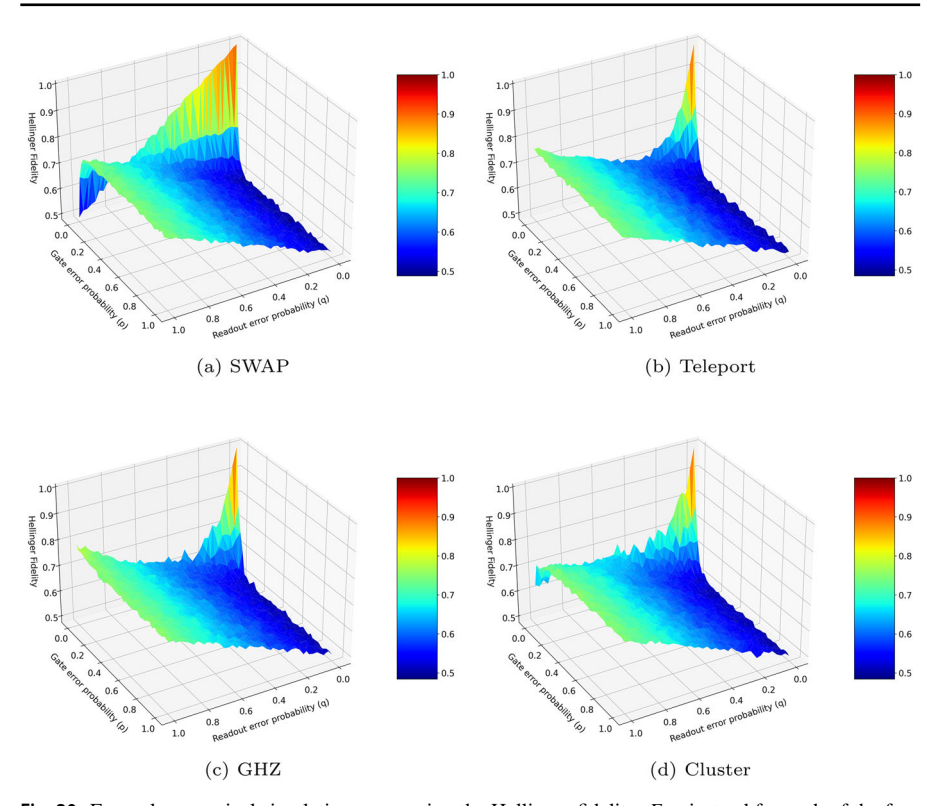


Fig. 20 Example numerical simulations measuring the Hellinger fidelity, F_H , instead for each of the four schemes for a seven-qubit circuit averaged over five randomly sampled initial states. The generated surface is composed of 1600 simulation data points (using 1024 shots)

nevertheless a useful measurement as it can serve as an analogy to some useful notion of fidelity, namely Hellinger fidelity.

Appendix F Success probability with individual Pauli-Noise

In Sect. 3.1, we performed numerical Qiskit simulations for success probabilities using the depolarizing error model from Eq. (1). Here we consider similar simulations (that is, keeping the same readout error model) using five-qubit circuits but replace our gate error model of gate error probability, p, with the following Pauli error model,

$$\mathcal{E}_i(\rho) = (1 - p)\rho + p(\sigma_i \rho \sigma_i) \tag{F1}$$

where $\sigma_1 = X$, $\sigma_2 = Y$, $\sigma_3 = Z$ gate. The respective simulation surface plots using $\mathcal{E}_1, \mathcal{E}_2$, and \mathcal{E}_3 are shown in Figs. 21, 22 and 23. From these, we can see that the kind of interplay between the errors can vary based on the gate error type. Figure 21 shows that the GHZ scheme is affected most by just Pauli-X errors and that the teleportation and SWAP scheme surfaces tend to have higher success probabilities despite high



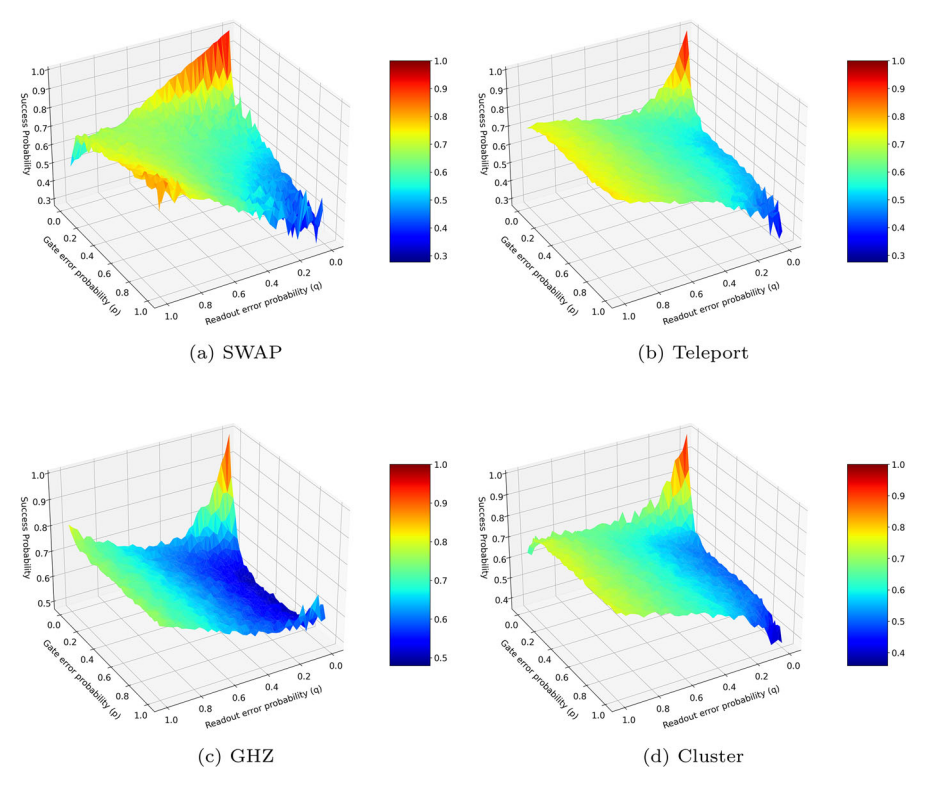


Fig. 21 Qiskit numerical simulations for a five-qubit successful state transfer using \mathcal{E}_1 with gate error probability p as the gate error model instead. Each data point is averaged over five randomly sampled initial states. The generated surface is composed of 1600 simulation data points (using 1024 shots each)

readout and gate errors—suggesting these schemes allow for better cancellation of the readout and Pauli-X error. Figure 22 then shows symmetry in the SWAP scheme in the face of Pauli-Y error (that is, both Pauli X and Z) perhaps owing to its own circuit gate symmetry. The remaining schemes perform similarly to the depolarizing noise case—not surprisingly as our depolarizing error model uses an equal mix of X, Y (which is just both X and Z), and Z. Lastly, Fig. 23 reveals that the SWAP scheme's success probability is least affected by Pauli-Z errors, followed by the Cluster scheme though with lots of variance between simulations. This suggests that the Cluster scheme's single, commuting, measurement-conditional Z gate is applied properly enough times due to the Pauli-Z interference. This advantage is not present for the worse dip in success probability with the teleportation and GHZ schemes, which have additional measurement-conditional X gates and so cannot leverage the 'constructive interference' seen in the Cluster scheme.



275 Page 32 of 36 B. Thotakura, T.-C Wei

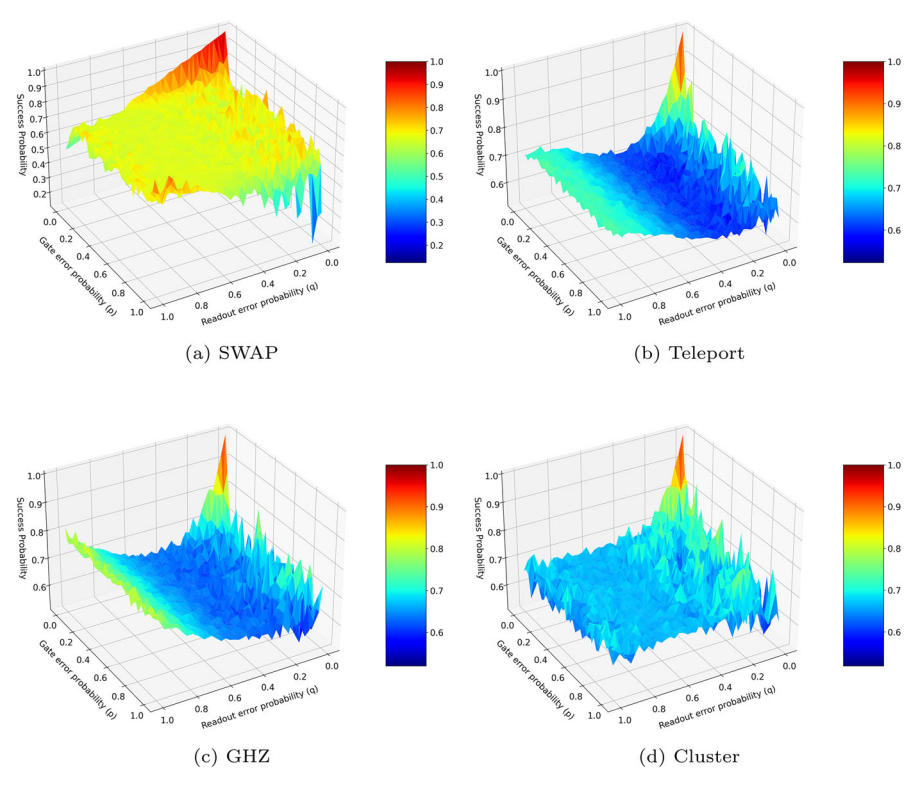


Fig. 22 Qiskit numerical simulations for a five-qubit successful state transfer using \mathcal{E}_2 with gate error probability p as the gate error model instead. Each data point is averaged over five randomly sampled initial states. The generated surface is composed of 1600 simulation data points (using 1024 shots each)



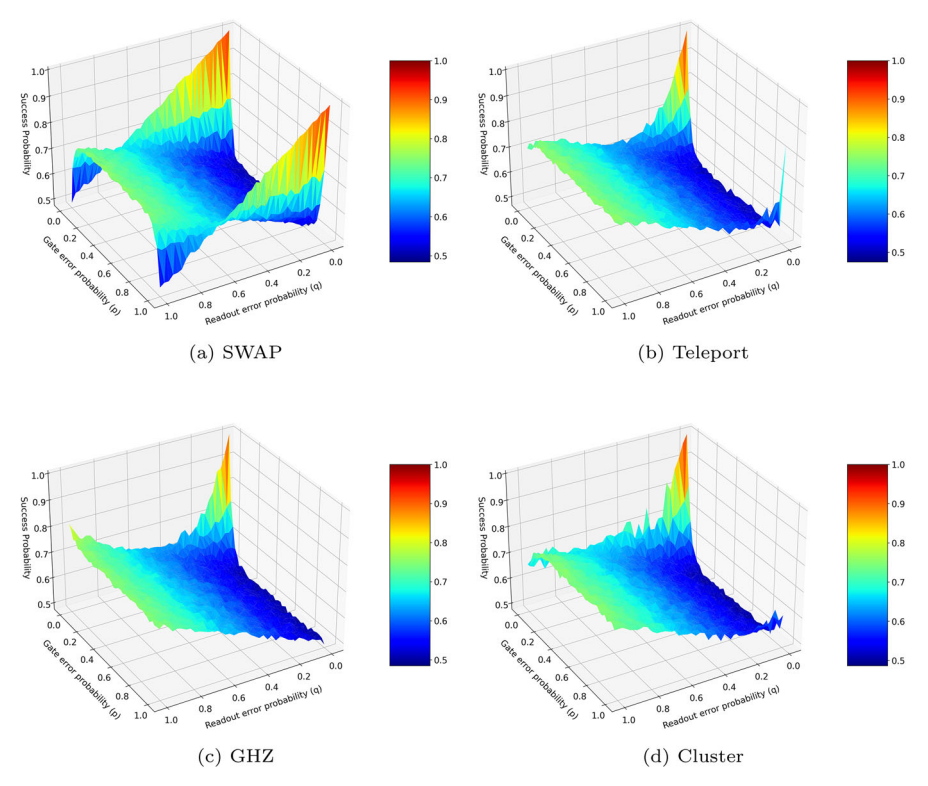


Fig. 23 Qiskit numerical simulations for a five-qubit successful state transfer using \mathcal{E}_3 with gate error probability p as the gate error model instead. Each data point is averaged over five randomly sampled initial states. The generated surface is composed of 1600 simulation data points (using 1024 shots each)

References

- 1. Kimble, H.J.: The quantum internet. Nature **453**(7198), 1023–1030 (2008)
- Bennett, C.H., Brassard, G., Crépeau, C., Jozsa, R., Peres, A., Wootters, W.K.: Teleporting an unknown quantum state via dual classical and Einstein–Podolsky–Rosen channels. Phys. Rev. Lett. 70, 1895– 1899 (1993). https://doi.org/10.1103/PhysRevLett.70.1895
- Pan, J.-W., Bouwmeester, D., Weinfurter, H., Zeilinger, A.: Experimental entanglement swapping: entangling photons that never interacted. Phys. Rev. Lett. 80(18), 3891 (1998)
- Duan, L.-M., Lukin, M.D., Cirac, J.I., Zoller, P.: Long-distance quantum communication with atomic ensembles and linear optics. Nature 414(6862), 413–418 (2001)
- 5. Pu, Y., Jiang, N., Chang, W., Yang, H., Li, C., Duan, L.: Experimental realization of a multiplexed quantum memory with 225 individually accessible memory cells. Nat. Commun. 8(1), 1–6 (2017)
- 6. Hermans, S., Pompili, M., Beukers, H., Baier, S., Borregaard, J., Hanson, R.: Qubit teleportation between non-neighbouring nodes in a quantum network. Nature **605**(7911), 663–668 (2022)
- Pompili, M., Hermans, S.L., Baier, S., Beukers, H.K., Humphreys, P.C., Schouten, R.N., Vermeulen, R.F., Tiggelman, M.J., dos Santos Martins, L., Dirkse, B., et al.: Realization of a multinode quantum network of remote solid-state qubits. Science 372(6539), 259–264 (2021)
- 8. van Leent, T., Bock, M., Fertig, F., Garthoff, R., Eppelt, S., Zhou, Y., Malik, P., Seubert, M., Bauer, T., Rosenfeld, W., et al.: Entangling single atoms over 33 km telecom fibre. Nature **607**(7917), 69–73 (2022)



275 Page 34 of 36 B. Thotakura, T.-C Wei

 Das, D., Dogra, S., Dorai, K.: Experimental construction of a w superposition state and its equivalence to the Greenberger–Horne–Zeilinger state under local filtration. Phys. Rev. A 92, 022307 (2015). https://doi.org/10.1103/PhysRevA.92.022307

- 10. Dorai, K., Suter, D.: Efficient implementations of the quantum fourier transform: an experimental perspective. Int. J. Quant. Inf. 3(02), 413–424 (2005)
- 11. Devra, A., Prabhu, P., Singh, H., Dorai, K.: Efficient experimental design of high-fidelity three-qubit quantum gates via genetic programming. Quantum Inf. Process. 17, 1–24 (2018)
- Dahlberg, A., Skrzypczyk, M., Coopmans, T., Wubben, L., Rozpędek, F., Pompili, M., Stolk, A., Pawełczak, P., Knegjens, R., de Oliveira Filho, J., et al.: A link layer protocol for quantum networks. In: Proceedings of the ACM Special Interest Group on Data Communication, pp. 159–173 (2019)
- van Dam, S.B., Humphreys, P.C., Rozpędek, F., Wehner, S., Hanson, R.: Multiplexed entanglement generation over quantum networks using multi-qubit nodes. Quant. Sci. Technol. 2(3), 034002 (2017)
- Kozlowski, W., Dahlberg, A., Wehner, S.: Designing a quantum network protocol. In: Proceedings of the 16th International Conference on Emerging Networking EXperiments and Technologies, pp. 1–16 (2020)
- Humphreys, P.C., Kalb, N., Morits, J.P., Schouten, R.N., Vermeulen, R.F., Twitchen, D.J., Markham, M., Hanson, R.: Deterministic delivery of remote entanglement on a quantum network. Nature 558(7709), 268–273 (2018)
- Rozpędek, F., Yehia, R., Goodenough, K., Ruf, M., Humphreys, P.C., Hanson, R., Wehner, S., Elkouss, D.: Near-term quantum-repeater experiments with nitrogen-vacancy centers: overcoming the limitations of direct transmission. Phys. Rev. A 99(5), 052330 (2019)
- Wehner, S., Elkouss, D., Hanson, R.: Quantum internet: a vision for the road ahead. Science 362(6412), 9288 (2018)
- Preskill, J.: Quantum computing in the NISQ era and beyond. Quantum 2, 79 (2018). https://doi.org/ 10.22331/q-2018-08-06-79
- Stephens, A.M., Huang, J., Nemoto, K., Munro, W.J.: Hybrid-system approach to fault-tolerant quantum communication. Phys. Rev. A 87(5), 052333 (2013)
- Campbell, E.T., Terhal, B.M., Vuillot, C.: Roads towards fault-tolerant universal quantum computation. Nature 549(7671), 172–179 (2017)
- Bourassa, J.E., Alexander, R.N., Vasmer, M., Patil, A., Tzitrin, I., Matsuura, T., Su, D., Baragiola, B.Q., Guha, S., Dauphinais, G., et al.: Blueprint for a scalable photonic fault-tolerant quantum computer. Quantum 5, 392 (2021)
- 22. Linke, N.M., Gutierrez, M., Landsman, K.A., Figgatt, C., Debnath, S., Brown, K.R., Monroe, C.: Fault-tolerant quantum error detection. Sci. Adv. 3(10), 1701074 (2017)
- Chen, Z., Satzinger, K.J., Atalaya, J., Korotkov, A.N., Dunsworth, A., Sank, D., Quintana, C., McEwen, M., Barends, R., Klimov, P.V., et al.: Exponential suppression of bit or phase flip errors with repetitive error correction. arXiv preprint arXiv:2102.06132 (2021)
- Cirac, J.I., Zoller, P., Kimble, H.J., Mabuchi, H.: Quantum state transfer and entanglement distribution among distant nodes in a quantum network. Phys. Rev. Lett. 78, 3221–3224 (1997). https://doi.org/ 10.1103/PhysRevLett.78.3221
- 25. Gisin, N., Thew, R.: Quantum communication. Nat. Photonics 1(3), 165–171 (2007)
- Orieux, A., Diamanti, E.: Recent advances on integrated quantum communications. J. Opt. 18(8), 083002 (2016)
- Cozzolino, D., Da Lio, B., Bacco, D., Oxenløwe, L.K.: High-dimensional quantum communication: benefits, progress, and future challenges. Adv. Quant. Technol. 2(12), 1900038 (2019)
- 28. Huang, N.-N., Huang, W.-H., Li, C.-M.: Identification of networking quantum teleportation on 14-qubit IBM universal quantum computer. Sci. Rep. 10(1), 1–12 (2020)
- Hillmich, S., Zulehner, A., Wille, R.: Exploiting quantum teleportation in quantum circuit mapping. In: 2021 26th Asia and South Pacific Design Automation Conference (ASP-DAC), pp. 792–797 (2021). IEEE
- Mooney, G.J., White, G.A., Hill, C.D., Hollenberg, L.C.: Whole-device entanglement in a 65-qubit superconducting quantum computer. Adv. Quant. Technol. 4(10), 2100061 (2021)
- 31. Behera, B.K., Seth, S., Das, A., Panigrahi, P.K.: Demonstration of entanglement purification and swapping protocol to design quantum repeater in IBM quantum computer. Quantum Inf. Process. **18**(4), 1–13 (2019)
- 32. Behera, B.K., Reza, T., Gupta, A., Panigrahi, P.K.: Designing quantum router in IBM quantum computer. Quantum Inf. Process. **18**(11), 1–13 (2019)



- 33. Das, S., Rahman, M., Majumdar, M., et al.: Design of a quantum repeater using quantum circuits and benchmarking its performance on an IBM quantum computer. Quantum Inf. Process. **20**(7), 1–17 (2021)
- 34. Palaiodimopoulos, N., Brouzos, I., Diakonos, F., Theocharis, G.: Fast and robust quantum state transfer via a topological chain. Phys. Rev. A 103(5), 052409 (2021)
- Chan, M.L., Aqua, Z., Tiranov, A., Dayan, B., Lodahl, P., Sørensen, A.S.: Quantum state transfer between a frequency-encoded photonic qubit and a quantum-dot spin in a nanophotonic waveguide. Phys. Rev. A 105(6), 062445 (2022)
- Serra, P., Ferrón, A., Osenda, O.: Almost perfect quantum state transfer on isotropic and anisotropic Heisenberg spin chains with tailored site dependent exchange couplings. Phys. Lett. A 449, 128362 (2022)
- 37. Qin, W., Wang, C., Long, G.L.: High-dimensional quantum state transfer through a quantum spin chain. Phys. Rev. A **87**(1), 012339 (2013)
- Qin, W., Li, J.-L., Long, G.-L.: High-dimensional quantum state transfer in a noisy network environment. Chin. Phys. B 24(4), 040305 (2015)
- 39. Yang, S., Song, Z., Sun, C.: Quantum state swapping via a qubit network with Hubbard interactions. Phys. Rev. B **73**(19), 195122 (2006)
- Štefaňák, M., Skoupỳ, S.: Perfect state transfer by means of discrete-time quantum walk on complete bipartite graphs. Quantum Inf. Process. 16, 1–14 (2017)
- Babukhin, D., Pogosov, W.: The effect of quantum noise on algorithmic perfect quantum state transfer on NISQ processors. Quantum Inf. Process. 21(1), 7 (2022)
- 42. Singh, H., Dorai, K., et al.: Evolution of tripartite entangled states in a decohering environment and their experimental protection using dynamical decoupling. Phys. Rev. A **97**(2), 022302 (2018)
- 43. Singh, H., Dorai, K., et al.: Constructing valid density matrices on an NMR quantum information processor via maximum likelihood estimation. Phys. Lett. A **380**(38), 3051–3056 (2016)
- Czarnik, P., Arrasmith, A., Coles, P.J., Cincio, L.: Error mitigation with Clifford quantum-circuit data. Quantum 5, 592 (2021)
- Giurgica-Tiron, T., Hindy, Y., LaRose, R., Mari, A., Zeng, W.J.: Digital zero noise extrapolation for quantum error mitigation. In: 2020 IEEE International Conference on Quantum Computing and Engineering (QCE), pp. 306–316 (2020). IEEE
- Temme, K., Bravyi, S., Gambetta, J.M.: Error mitigation for short-depth quantum circuits. Phys. Rev. Lett. 119(18), 180509 (2017)
- ANIS, M.S., et al.: Qiskit: an open-source framework for quantum computing (2021). https://doi.org/ 10.5281/zenodo.2573505
- Munro, W.J., Azuma, K., Tamaki, K., Nemoto, K.: Inside quantum repeaters. IEEE J. Sel. Top. Quantum Electron. 21(3), 78–90 (2015)
- 49. Greenberger, D.M., Horne, M.A., Zeilinger, A.: Going beyond bell's theorem. Bell's theorem, quantum theory and conceptions of the universe, 69–72 (1989)
- Greenberger, D.M., Horne, M.A., Shimony, A., Zeilinger, A.: Bell's theorem without inequalities. Am. J. Phys. 58(12), 1131–1143 (1990)
- Briegel, H.J., Raussendorf, R.: Persistent entanglement in arrays of interacting particles. Phys. Rev. Lett. 86(5), 910 (2001)
- 52. Nielsen, M.A.: Cluster-state quantum computation. Rep. Math. Phys. 57(1), 147–161 (2006)
- Sangouard, N., Simon, C., de Riedmatten, H., Gisin, N.: Quantum repeaters based on atomic ensembles and linear optics. Rev. Mod. Phys. 83, 33–80 (2011). https://doi.org/10.1103/RevModPhys.83.33
- Garcia-Escartin, J.C., Chamorro-Posada, P.: Equivalent quantum circuits. arXiv preprint arXiv:1110.2998 (2011)
- 55. Georgopoulos, K., Emary, C., Zuliani, P.: Modeling and simulating the noisy behavior of near-term quantum computers. Phys. Rev. A **104**(6), 062432 (2021)
- Nielsen, M.A., Chuang, I.L.: Quantum Computation and Quantum Information: 10th Anniversary Edition, 10th edn. Cambridge University Press, USA (2011)
- 57. Pedregosa, F., Varoquaux, G., Gramfort, A., Michel, V., Thirion, B., Grisel, O., Blondel, M., Prettenhofer, P., Weiss, R., Dubourg, V., Vanderplas, J., Passos, A., Cournapeau, D., Brucher, M., Perrot, M., Duchesnay, E.: Scikit-learn: machine learning in Python. J. Mach. Learn. Res. 12, 2825–2830 (2011)
- 58. Inc., P.T.: Collaborative Data Science. https://plot.ly
- Sun, J., Yuan, X., Tsunoda, T., Vedral, V., Benjamin, S.C., Endo, S.: Mitigating realistic noise in practical noisy intermediate-scale quantum devices. Phys. Rev. Appl. 15(3), 034026 (2021)



275 Page 36 of 36 B. Thotakura, T.-C Wei

 Coopmans, T., Knegjens, R., Dahlberg, A., Maier, D., Nijsten, L., de Oliveira Filho, J., Papendrecht, M., Rabbie, J., Rozpędek, F., Skrzypczyk, M., et al.: Netsquid, a network simulator for quantum information using discrete events. Commun. Phys. 4(1), 1–15 (2021)

- Maciejewski, F.B., Zimborás, Z., Oszmaniec, M.: Mitigation of readout noise in near-term quantum devices by classical post-processing based on detector tomography. Quantum 4, 257 (2020)
- Chen, Y., Farahzad, M., Yoo, S., Wei, T.-C.: Detector tomography on IBM quantum computers and mitigation of an imperfect measurement. Phys. Rev. A 100(5), 052315 (2019)
- 63. Hardy, L., Song, D.D.: Universal manipulation of a single qubit. Phys. Rev. A 63(3), 032304 (2001)
- Bowdrey, M.D., Oi, D.K., Short, A.J., Banaszek, K., Jones, J.A.: Fidelity of single qubit maps. Phys. Lett. A 294(5–6), 258–260 (2002)
- Koch, J., Terri, M.Y., Gambetta, J., Houck, A.A., Schuster, D.I., Majer, J., Blais, A., Devoret, M.H., Girvin, S.M., Schoelkopf, R.J.: Charge-insensitive qubit design derived from the cooper pair box. Phys. Rev. A 76(4), 042319 (2007)
- Mantri, A., Demarie, T.F., Fitzsimons, J.F.: Universality of quantum computation with cluster states and (x, y)-plane measurements. Sci. Rep. 7(1), 42861 (2017)
- 67. Luo, S., Zhang, Q.: Informational distance on quantum-state space. Phys. Rev. A 69(3), 032106 (2004)

Publisher's Note Springer Nature remains neutral with regard to jurisdictional claims in published maps and institutional affiliations.

Springer Nature or its licensor (e.g. a society or other partner) holds exclusive rights to this article under a publishing agreement with the author(s) or other rightsholder(s); author self-archiving of the accepted manuscript version of this article is solely governed by the terms of such publishing agreement and applicable law

